minerals

MDPI

Article

The Chemical Evolution from Older (323–318 Ma) towards Younger Highly Evolved Tin Granites (315–314 Ma)—Sources and Metal Enrichment in Variscan Granites of the Western Erzgebirge (Central European Variscides, Germany)

Marion Tichomirowa [1,*], Axel Gerdes [2], Manuel Lapp [3], Dietmar Leonhardt [3] and Martin Whitehouse [4]

[1] Institut für Mineralogie, TU Bergakademie Freiberg, Brennhausgasse 14, D-09599 Freiberg/Sachsen, Germany
[2] Institut für Geowissenschaften, Goethe Universität Frankfurt, Altenhoeferallee 1, D-60438 Frankfurt am Main, Germany; gerdes@em.uni-frankfurt.de
[3] Saxonian Geological Survey, Halsbrücker Str. 31a, D-09599 Freiberg, Germany; Manuel.Lapp@smul.sachsen.de (M.P.); leo-freib@t-online.de (D.L.)
[4] Swedish Museum of Natural History, Box 50007, SE-1045 Stockholm, Sweden; martin.whitehouse@nrm.se
* Correspondence: tichomir@mineral.tu-freiberg.de; Tel.: +49-3731-393528

Received: 23 October 2019; Accepted: 10 December 2019; Published: 11 December 2019

Abstract: The sources and critical enrichment processes for granite related tin ores are still not well understood. The Erzgebirge represents one of the classical regions for tin mineralization. We investigated the four largest plutons from the Western Erzgebirge (Germany) for the geochemistry of bulk rocks and autocrystic zircons and relate this information to their intrusion ages. The source rocks of the Variscan granites were identified as high-grade metamorphic rocks based on the comparison of Hf-O isotope data on zircons, the abundance of xenocrystic zircon ages as well as Nd and Hf model ages. Among these rocks, restite is the most likely candidate for later Variscan melts. Based on the evolution with time, we could reconstruct enrichment factors for tin and tungsten starting from the protoliths (575 Ma) that were later converted to high-grade metamorphic rocks (340 Ma) and served as sources for the older biotite granites (323–318 Ma) and the tin granites (315–314 Ma). This evolution involved a continuous enrichment of both tin and tungsten with an enrichment factor of ~15 for tin and ~7 for tungsten compared to the upper continental crust (UCC). Ore level concentrations (>10–100 times enrichment) were achieved only in the greisen bodies and dykes by subsequent hydrothermal processes.

Keywords: tin granites; crustal melts; S-type granites; zircon; hafnium isotopes; oxygen isotopes; greisen; Erzgebirge; granite source

1. Introduction

At the end of the Variscan orogeny, voluminous granite plutons intruded the European upper crust. In some areas—like in the Erzgebirge or southwestern England—these granites are associated with extreme enrichments of elements such as Sn, W, or Mo, and with the formation of large ore deposits. "Tin granites" are usually regarded as S-type granites that crystallized under reduced conditions [1,2]. However, there is no consensus about the source rocks of such granites and their critical enrichment processes. For the late Variscan Cornubian Batholith, the melting of feldspathic greywackes has been proposed as the main protolith for these granites [2]. For the Erzgebirge granites, a mixture of sedimentary rocks (meta-pelites/shales) with evolved magmatic sources (quartzo-feldspathic rocks)

has been supposed as protoliths [1,3–5]. In addition, intense weathering of Early Paleozoic sediments was postulated to be necessary for the Sn enrichment [6,7].

In the Erzgebirge, sedimentary and magmatic host rocks of Variscan granites were subducted to various depths and are now exposed at the surface (low pressure, middle pressure, high pressure rocks). These rocks were intensely studied by petrology, geochemistry, and geochronology [8–17]. Therefore, the Erzgebirge is an ideal region for comparing geochemical and geochronological fingerprints of potential source rocks with that of granites. In addition, the sequence of Variscan granite intrusions was recently established by high-precision U-Pb zircon CA-ID-TIMS dating for the four largest intrusions in the Western Erzgebirge [18]. Based on these studies, the geochemical evolution of Variscan granites can be analyzed for a time span of ~8–9 Ma: starting from early unevolved biotite granites to highly specialized Li-mica bearing tin granites. Here, we use bulk rock geochemistry (elements, Nd, and Sr isotopes) in combination with zircon geochemistry (Hf and O isotopes, trace elements) to reconstruct the temperature and sources of melt formation. We discuss what information can be inferred from various geochemical proxies (i) from bulk rocks, and (ii) from zircon crystals that precipitated from the melt. This allows us to reconstruct the sources of granites as well as enrichment processes that finally led to ore level concentrations of Sn and W in ore bodies and test various suggestions necessary for ore level enrichments, e.g., [6,7].

2. Regional Geology and Previous Geochemistry

The Erzgebirge is part of the Variscan orogenic belt and is located at the northern margin of the Bohemian Massif at the border between Germany and the Czech Republic (Figure 1a). It forms a large anticlinal structure (80 x 40 km) made up of felsic amphibolite-facies gneisses with frequent lenses of eclogite, amphibolite, and felsic granulites [19]. Some of these eclogite- and granulite-facies rocks were buried to UHP conditions at mantle depth (evidence from coesite and diamond: e.g., [20,21]). The ages suggested for peak (U)HP metamorphism cover a range from 360 to 330 Ma [9,10,15,22,23]. Petrological studies discriminated several units with different P-T histories [9,11,24], which together represent a tectonic stack of different crustal segments formed during the Variscan subduction and continent-continent collision [25]. Gneisses form the core while mica schists and phyllites are located at the rim of the antiformal structure of the Erzgebirge [19].

The Variscan granites of the Erzgebirge form various larger and smaller bodies within their metamorphosed host rocks (Figure 1). In the Western Erzgebirge, the granites intruded at shallow depths (3–6 km below the surface; [26]) while in the Eastern Erzgebirge volcanic magmatites also occur. The whole Erzgebirge is underlain by a negative Bouguer anomaly implying the presence of granites at least for several km below the surface [27]. Several boreholes confirmed the presence of granites at depths under meta-sediments exposed at the surface [28].

Variscan granites in the Erzgebirge traditionally have been subdivided into the "mountain granites" (Gebirgsgranite) and the "ore mountain granites" (Erzgebirgsgranite), indicating the close relationship of the latter to ore formation (Figure 1c) [29]. Later, these two groups were assigned to "older" and "younger" intrusive complexes (OIC and YIC, [30,31]). These two groups of granite have clear differences in their bulk rock geochemistry (Figure 1c) [32].

In the Western Erzgebirge, the largest intrusion is the Eibenstock/Nejdek (EIB) pluton, that is in its German part a typical representative of the highly specialized tin granites, while the nearby Kirchberg (KIB) and Bergen (BER) plutons, as well as the smaller granite outcrops near Aue and Schwarzenberg (ASB), are assigned to the less evolved granite group 1 (Figure 1) [33]. These granites intruded mainly into Ordovician phyllites and belong to the first Variscan intrusion period (323–314 Ma) [18]. A later Variscan period of magmatic activity is represented by subvolcanic dykes and the likely coeval small granite intrusions of Eichigt-Schönbrunn [34]: 297 ± 8 Ma, SHRIMP; [35]: 305–295 Ma, EMP monazite and Ar-Ar dating). This second period of magmatic activity is not considered in this paper.

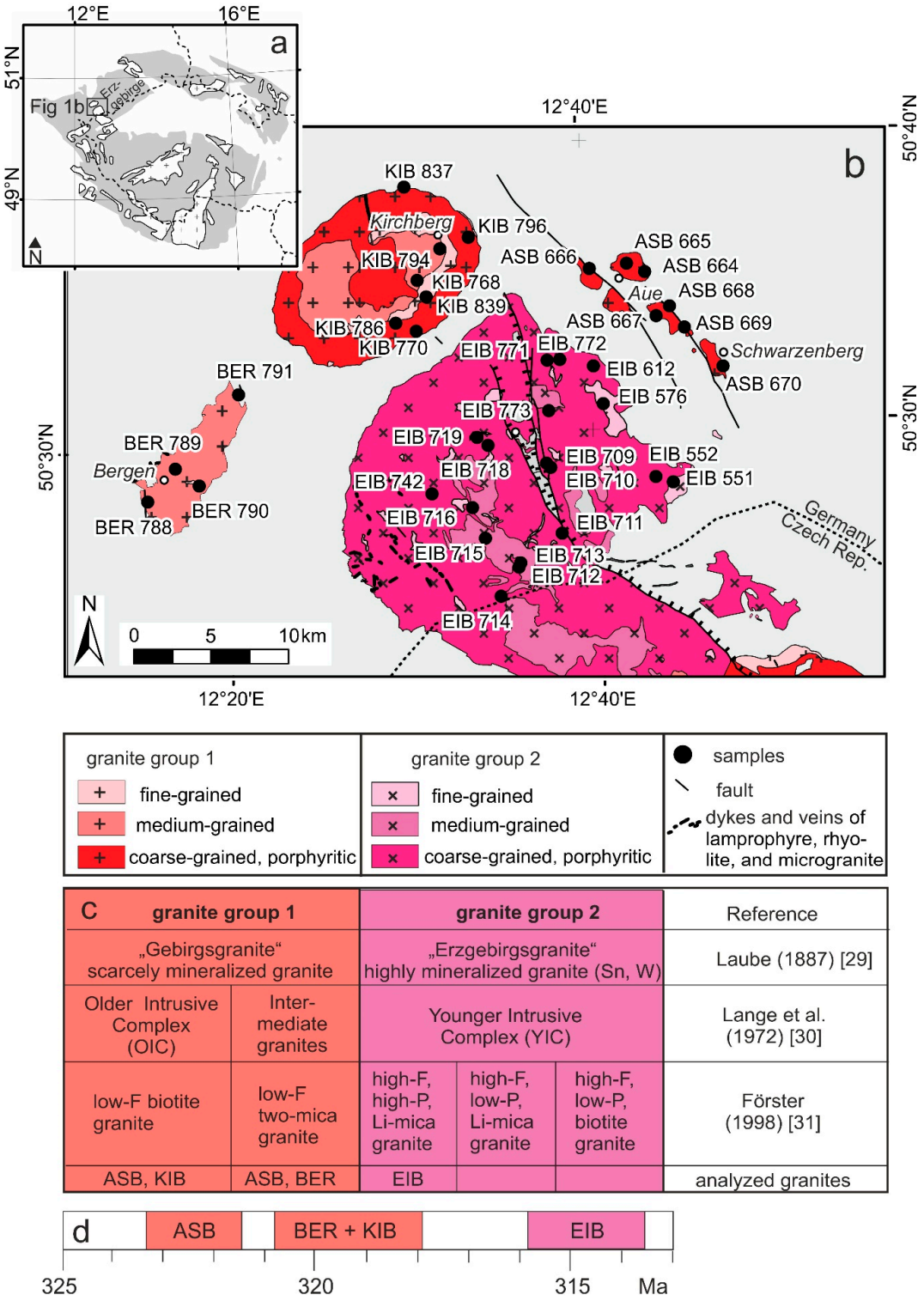

Figure 1. Geological map with sample locations in the Western Erzgebirge, Germany. (**a**) The inset shows the location of the study area within the Bohemian Massif. (**b**) The four largest plutons/suites of Variscan granites in the Western Erzgebirge/Krušné Hory are shown: Aue-Schwarzenberg (ASB), Bergen, (BER), Eibenstock (EIB), and Kirchberg (KIB). EIB belongs in the German part to granite group 2 while the three other plutons belong to granite group 1. (**c**) Classification of Variscan granites from the Erzgebirge according to different authors using distinct parameters, and assignment of analyzed granite plutons to these granite groups. (**d**) Intrusion periods of the four plutons determined by zircon U-Pb CA-ID-TIMS [18].

Several petrological varieties of granites occur in the Erzgebirge, e.g., biotite granites, two-mica granites, and Li-mica granites. Each pluton is composed of several non-deformed textures: coarse-grained porphyritic (main intrusive phase), medium-grained (sometimes porphyritic), fine-grained porphyritic or fine-grained equigranular, fine-grained aplitic dykes [36] (Figure 1). According to their major mineral composition (quartz, alkali feldspars, plagioclase), the rocks represent mainly monzo-granites and granodiorites [31] and are assigned to S-type granites [36]. The EIB granite (second group) has lower abundances of plagioclase compared to ASB, BER, and KIB. In the Western Erzgebirge, the first and second granite group differ in their petrological composition (biotite and two-mica granites versus Li-mica) and their geochemistry (low fluorine versus high fluorine contents; Figure 1c). In [5], the ASB was divided into two subgroups, the northern Aue subgroup that occurs as biotite granites and the southern Schwarzenberg subgroup that is composed of two-mica granites.

An extensive geochronological database exists but all previous dating did not reveal a clear age difference between both granite groups because of relatively large errors (≥1%) of applied dating methods (see compilation of age data in [18]). The sequence of intrusions was only recently established by precise and accurate CA-ID-TIMS zircon dating [18]: the ASB granites intruded first (~323–322 Ma) followed a few Ma later by the granites from BER and KIB (~320–318 Ma). The highly evolved F- and Li-rich tin granites from Eibenstock intruded considerably later at ~315–314 Ma (Figure 1d) [18].

Granites from the Erzgebirge/Krušné Hory were intensely studied by geochemistry, and specifically the granites from ASB, BER, EIB and KIB, e.g., [1,3–5,37–39]. The strong enrichment of rare alkalis (Li, Rb, Cs), lithophiles (Sn, W, Nb, Ta), fluorine, and uranium in the Li-mica granites was explained by a combination of (a) evolved melt sources, (b) extreme degrees of magma fractionation, and (c) superposition of late- to post-magmatic, auto-metasomatic processes [38]. Förster et al. [37] proposed a classification into five different granite groups by geochemistry: (1) low-F biotite granites; (2) low-F, two-mica granites; (3) high-F, high-P_2O_5 Li-mica granites; (4) high-F, low-P_2O_5 Li-mica granites; and (5) high-F, low-P_2O_5 biotite granites (Figure 1c). These authors [37] have shown for the first time that ASB, KIB, and BER granites have lower F contents compared to all samples from EIB so that the F-P_2O_5 diagram can be used as a discrimination diagram. The authors stated that each of these five groups underwent an individual igneous evolution and used the reciprocal value of the titanium concentration ($1/TiO_2$) as the parameter for the degree of fractionation in the melt. They also showed that the greisen from each group and their host granites have similar tendencies in F- and P_2O_5-concentrations.

Breiter et al. [1] explained the chemical trends of the granites by fractional crystallization and related the formation of Sn-W deposits to late-magmatic–early post-magmatic mineralization, with fractional crystallization, fluid-melt immiscibility, hydro-fracturing, and fluid-rock interaction as the main enrichment processes. In contrast, Stemprok et al. [40] explained the trends in bulk rock geochemistry of these upper crustal magmas by mixing of (i) early crystallized phenocrysts and (ii) melt that later crystallized as fine- to medium-grained matrix of these granites.

Studies of melt inclusions in Variscan granites from the Erzgebirge yielded shallow emplacement depths (3–6 km below surface), crystallization temperatures near 700 °C, and extreme volatile enrichment from the early, higher-temperature crystallization stages (~3 equiv. wt % H_2O) to the latest melt fractions (~10 equiv. wt % H_2O) [26]. The melt- and fluid-inclusion studies [26,41–43] demonstrated that the latest melt stages were extremely enriched in elements like Sn, F, P, Li, Rb, Cs, Nb, Ta, Be, locally in U, Th, and W, and had a very high enrichment in elements that decrease melt viscosity (F, P, B). Although F is usually partitioned into the melt, it was proposed to separate into the fluids at the latest stages of the magmatic evolution, leading to further enrichment of Sn [44]. This is in agreement with the thermodynamic analysis of Ca-enriched peraluminous granites, showing that decomposition of topaz and decalcification of plagioclase caused by hydrothermal fluids results in fluorite formation [45]. Inclusion studies, as well as detailed chemical investigations of quartz and feldspar [3,46], showed that the investigated rocks may contain several generations of melt and minerals.

Despite the extensive literature on the granites from the Erzgebirge, there is little consensus on their protoliths. For the Erzgebirge/Krušné Hory, most authors proposed a mix of two sources: (i) a sedimentary source (pelites, shales) and (ii) a "fertile" or "evolved" source like quartzo-feldspathic rocks (metagreywackes and orthogneisses) e.g., [4,39]. In addition, other sources like a juvenile component (volcanic rocks or former oceanic crust [47] or lower crustal sources [48]) have been proposed. In contrast to Cornubian granites where greywackes are suggested as the main sedimentary protolith [2], mainly shales [3,4] have been assumed as the sedimentary source for granites in the Erzgebirge. Specifically, highly weathered Ordovician shales from the Frauenbach Group have been suggested [6]—because of their high K_2O/Na_2O ratios—as the most potential sedimentary source rock. The suggestion of a mix of two sources is mainly based on Sr- and Nd-isotope data from granitic bulk rocks that plot between Paleozoic sediments and more juvenile volcanic/volcanogenic clastic sediments from Saxothuringia [36]. However, the initial $^{87}Sr/^{86}Sr$ ratios calculated from bulk rock data from the evolved YIC granites are very questionable because they often resulted in too low and erroneous values (sometimes <0.7000) because of their extremely high Rb/Sr-ratios [36]. This was interpreted as evidence for a poly-stage evolution and the disturbance of the Rb-Sr system [36]. Li- and B-isotopes did not provide specific information as source tracers for the Variscan granites [47].

3. Samples and Analytical Methods

3.1. Samples

Samples were taken from the four largest plutons/suites of Variscan granites in the German part of the Erzgebirge: from the Aue-Schwarzenberg (ASB), the Bergen (BER), the Kirchberg (KIB), and the Eibenstock (EIB) granite. For each pluton/suite 4–18 samples are analyzed representing different textural varieties (Figure 1; Table 1). Several of these samples have been formerly analyzed by zircon U-Pb dating (LA-ICP-MS, SHRIMP, CA-ID-TIMS) [18]. Table 1 gives an overview of samples, their textures, and applied methods.

3.2. Bulk Rock Geochemistry

Major and trace element contents for whole-rock samples were analyzed at Activation Laboratories (Actlabs Canada; "4 Litho" research analytical protocol) by Fusion-ICP and Fusion-MS, respectively. Samples were fused with lithium metaborate/tetraborate and afterward diluted and analyzed by Perkin Elmer Sciex ELAN 6000, 6100 or 9000 ICP/MS. Three blanks and five controls (three before the sample group and two after) are analyzed per group of samples. Duplicates are fused and analyzed every 15 samples. The instrument is recalibrated every 40 samples. Reproducibility is better than 1% for major elements and better than 5% for trace elements based on analyses of certified standards.

3.3. Bulk Rock Nd Isotope Ratios

About 200 milligrams of powder from whole-rock were dissolved in 50% HF-12N HNO_3, then attacked with 8N HNO_3 and finally with 6N HCl. Samarium and neodymium were separated by ion-exchange resins. The isotope ratios were measured on a Finnigan MAT 262 spectrometer and the quoted errors are given at the 2σ level. Concentrations of Sm and Nd were obtained by isotope dilution. The $^{143}Nd/^{144}Nd$ ratios were normalized to $^{146}Nd/^{144}Nd = 0.7219$ [49]. Sm-Nd model ages were calculated using the depleted mantle model (T_{DM}) [49]. The mean value for $^{143}Nd/^{144}Nd$ of the standard JNdi was 0.512098 ± 0.000010 (n = 8).

Table 1. Sample locations, description, and applied methods.

Sample Name	Location Name	Latitude (N)	Longitude (E)	Rock Description	Bulk Rock Geochemistry	$^{143}Nd/^{144}Nd$ Bulk Rock	$^{87}Sr/^{86}Sr$ Bulk Rock *	$\delta^{18}O$ of Zircon	$^{176}Hf/^{177}Hf$ of Zircon	Trace Elements in Zircon
(a) granites from Aue-Schwarzenberg (ASB, Western Erzgebirge)										
ASB 664	Niederpfannenstiel	12°43′20.01″	50°35′15.60″	Medium grained (granite Aue)	X					
ASB 665	Aue	12°42′2.07″	50°35′40.02″	Medium grained porphyritic	X	X		X	X	
ASB 666	Auerhammer	12°39′59.92″	50°35′32.00″	Coarse grained porphyritic	X	X	X	X	X	
ASB 667	Schalenberg, Lauter	12°43′44.11″	50°33′53.24″	Fine grained (granite Lauter)	X					
ASB 668	Lauter	12°44′7.70″	50°34′3.77″	Medium grained porphyritic	X	X		X	X	
ASB 669	Lauterer Förstel	12°45′23.15″	50°33′15.38″	Fine grained (granite Neuwelt)	X					
ASB 670	Schwarzenberg	12°47′0.49″	50°32′1.59″	Medium grained	X	X	X	X	X	
(b) granites from the Bergen pluton (BER, Western Erzgebirge)										
BER 788	quarry Streuberg	12°15′37.46″	50°28′13.11″	Coarse-grained porphyritic	X	X		X	X	
BER 789	quarry NW Trieb	12°17′11.93″	50°29′18.27″	medium grained	X	X		X	X	
BER 790	quarry SE Trieb	12°18′26.78″	50°28′41.18″	fine grained	X	X		X	X	
BER 791	quarry Kuxenberghäuser	12°20′37.46″	50°31′45.30″	medium grained	X	X		X	X	
(c) granites from the Kirchberg pluton (KIB, Western Erzgebirge)										
KIB 768	Giegengrün	12°30′46.87″	50°35′22.50″	fine grained (slightly porphyritic)	X					
KIB 770	Crinitzberg	12°30′35.93″	50°33′47.88″	coarse grained porphyritic	X					
KIB 786	Obercrinitz	12°29′25.93″	50°33′59.35″	fine grained	X	X		X	X	
KIB 794	Leutersbach	12°32′0.06″	50°36′28.20″	fine grained (slightly porphyritic)	X	X	X	X	X	
KIB 796	E Saupersdorf	12°33′44.07″	50°36′48.75″	coarse grained porphyritic	X	X	X	X	X	
KIB 837	Schelmberg	12°32′9.30″	50°38′22.83″	coarse grained porphyritic	X					
KIB 839	SW Giegengrün	12°30′42.22″	50°34′52.75″	coarse grained porphyritic	X					
(d) granites from the Eibenstock pluton (EIB, Western Erzgebirge)										
EIB 612	Falkenstein	12°39′56.10″	50°32′12.65″	fine grained greisen	X	X	X	X	X	X
EIB 709	Kamelfelsen	12°37′23.18″	50°28′56.05″	coarse grained porphyritic (type Eibenstock)	X					
EIB 710	Kamelfelsen	12°37′25.23″	50°28′57.66″	fine grained	X					
EIB 712	Weiterswiese	12°35′54.99″	50°25′41.67″	medium grained granite (type Blauenthal)	X	X		X	X	
EIB 713	Weiterswiese	12°35′54.99″	50°25′41.67″	fine grained greisen	X					
EIB 714	quarry Seerbächel	12°34′24.89″	50°24′25.09″	medium grained porphyritic (type Walfischkopf)	X		X			
EIB 718	Krinitzberg	12°34′4.82″	50°29′37.52″	fine grained porphyritic (type Krinitzberg)	X	X	X	X	X	
EIB 719	Walfischkopf	12°33′30.57″	50°29′58.73″	fine grained porphyritic (type Walfischkopf)	X	X	X	X	X	X
EIB 551	Rabenberg	12°44′11.22″	50°28′11.11″	fine grained	X					
EIB 552	Erlabrunn	12°43′30.24″	50°28′17.03″	coarse grained porphyritic (type Eibenstock)	X					

Table 1. *Cont.*

Sample Name	Location Name	Latitude (N)	Longitude (E)	Rock Description	Bulk Rock Geochemistry	$^{143}Nd/^{144}Nd$ Bulk Rock	$^{87}Sr/^{86}Sr$ Bulk Rock *	$\delta^{18}O$ of Zircon	$^{176}Hf/^{177}Hf$ of Zircon	Trace Elements in Zircon
EIB 576	Pechtute/Bockau	12°41′11.44″	50°31′22.66″	fine to medium grained porphyritic	X					
EIB 711	Schöne Aussicht/Wildenthal	12°37′50.52″	50°26′25.73″	coarse grained porphyritic (type Eibenstock)	X					
EIB 715	Blechhammer	12°33′49.70″	50°26′59.60″	fine grained	X					
EIB 716	Tannenberg	12°33′28.72″	50°27′47.49″	medium grained granite (type Blauenthal)	X					
EIB 742	Schönheide	12°31′3.37″	50°28′26.19″	fine-grained	X					
EIB 771	Steinberg	12°38′5.50″	50°32′28.12″	fine grained (slightly porphyritic)	X					
EIB 772	Burkhardtsgrün	12°38′50.63″	50°32′22.53″	medium grained porphyritic (type Walfischkopf)	X					
EIB 773	quarry Blauenthal	12°37′58.74″	50°31′0.45″	medium grained granite (type Blauenthal)	X					

* according to [18].

3.4. Zircon Geochemistry: Hf Isotope Ratios, O Isotope Ratios, Trace Elements

Hafnium isotopes were measured on a Thermo-Finnigan Neptune multi-collector ICP-MS coupled to a Resonetics 193nm ArF excimer laser (CompexPro 102, Coherent) system at Goethe-University Frankfurt (GUF) [50]. Spots of 40 to 60 μm in diameter were drilled with a repetition rate of 5.5 Hz and an energy density of 5 J/cm^2 during 55 s of data acquisition. All data were adjusted relative to the JMC475 standard (^{176}Hf/^{177}Hf = 0.282160) and quoted uncertainties are quadratic additions of the within run precision of each analysis and the reproducibility of JMC475 (2 SD = 0.0028%, n = 6). We verified the accuracy and external reproducibility by repeated analysis of two reference zircons, Temora and GJ-1. They yielded ^{176}Hf/^{177}Hf ratios of 0.282689 ± 0.000023 (2 SD, n = 11 for Temora), 0.282012 ± 0.000014 (2 SD, n = 8 for GJ-1). This is in perfect agreement with previously published results, e.g., [50,51] and with the LA-MC-ICPMS long-term average (2006–2012) of GJ-1 (0.282010 ± 0.000025; n > 800) reference zircon at GUF.

Zircon oxygen isotopes were measured with the Cameca IMS 1280 multicollector ion microprobe at the Swedish Museum of Natural History [52], utilizing a ~2 nA Cs^+ primary ion beam together with a normal incidence low-energy electron gun for charge compensation, medium field magnification (~80x), and two Faraday detectors (channels L2 and H2) at a typical mass resolution of ~2500. Measurements were performed in pre-programmed chain analysis mode with automatic field aperture and entrance slit, centered on the ^{16}O signal. The magnetic field was locked using NMR regulation for the entire analytical session. Each data-acquisition run comprised a 20 × 20 μm pre-sputter to remove the Au layer, followed by the centering steps, and 64 seconds of data integration performed using a non-rastered ~10 × 10 μm spot. In the measurement chain, every set of four unknowns was followed by two bracketing analyses on the 91500 standard zircon. A δ^{18}O value of +9.86‰ (SMOW) [53] was assumed for the 91500 zircon in data normalization, and small linear-drift corrections were applied to each session. External reproducibility of ±0.3‰ (1 SD) based on measurements on the standards was propagated into the overall uncertainty for each analysis.

Measurements of trace elements, including Rare Earth Elements (REE) in selected zircon grains, were made on the CAMECA ims-4f ion microprobe at Yaroslavl Institute of Microelectronics and Informatics (Russian Academy of Science). Measurements of P, Ca, Ti, Y, Nb, Ba, REE, Hf, Th, U were made with a spot area of ~25 μm. Intensities were calibrated against 610 NIST basalt glass, and isobar interferences were corrected according to [54]. For REE analyses, overall uncertainties are better than 15%, and for other trace elements, better than 5%.

4. Results

4.1. Bulk Rock Geochemistry

Data are given in Table S1. Selected diagrams are presented in Figure 2. All plutons show wide variations in their concentrations that often form trend lines in Harker diagrams (Figure 2a) or against TiO_2 (Figure 2b). In accordance with previously published data e.g., [1,3–5,32] SiO_2 correlates negatively with MgO, Al_2O_3, TiO_2, and CaO, V, Zr, Ba. The correlated decrease of MgO, TiO_2, and CaO indicates combined fractionation of biotite with plagioclase. The observed trend in Ba-Sr-Rb diagrams (Figure 2c shows Ba vs. Sr) also reflects this combined fractionation of biotite with plagioclase. The rock texture (mainly the occurrence, abundance, and size of K-feldspar megacrysts) is related to element concentrations in bulk rocks as all porphyritic varieties plot at the low SiO_2 end (Figure 2).

There are some differences between plutons, especially for KIB samples, that often have higher Th, REE, Zr concentrations, and lower FeO/MgO and A/CNK ratios. Based on these differences, KIB was classified as A-type granites [39]. KIB granites tend to lower A/CNK values and can be classified as high K calcalkaline granites. The F-rich EIB granites have a clearly different chemical composition compared to all OIC in accordance with previously published data: e.g., high F, Rb, Cs, low Ba, Sr, TiO_2 concentrations (Figure 2) [1,3–5,32].

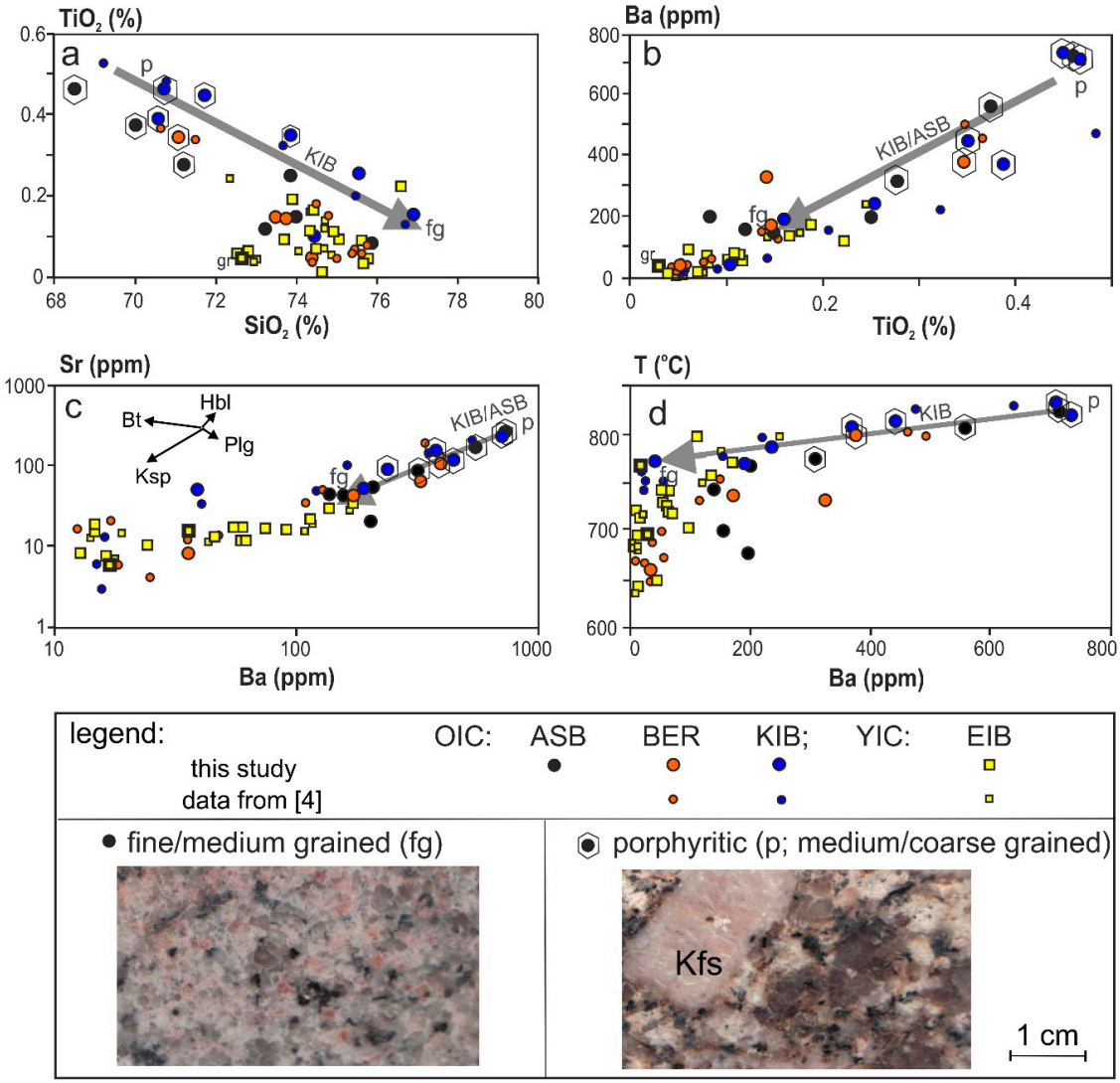

Figure 2. Bulk rock geochemistry. (**a**) SiO_2 versus TiO_2, (**b**) TiO_2 versus Ba, (**c**) Ba versus Sr, (**d**) Ba versus calculated zircon saturation temperature [55]. fg—fine/medium grained, p—porphyritic with large phenocrysts of K-feldspars (Kfs).

We have calculated temperatures from bulk rock data according to two published approaches. Inherited zircons are extremely scarce [18] and this allows us to calculate zircon saturation temperatures as indications for melt temperatures [55]. The mean zircon saturation temperatures are 735 °C for BER and EIB, 760 °C for ASB, and 800 °C for KIB (Table S1). In addition, we have applied the Al_2O_3/TiO_2 thermometer for bulk rock data [56] and obtained the highest mean melt temperatures (~880 °C) for KIB, followed by ASB (~850 °C), BER (~790 °C) while EIB granites yielded the lowest calculated temperatures for (~740 °C; Table S1).

Sm and Nd isotope data of bulk rocks are presented in Table 2. All samples yielded epsilon Nd values in a narrow range from −3.0 to −5.6 consistent with previously published data [4,5].

Table 2. Sm-Nd isotope data. T DM calculated according to [49].

Sample Number	Sm ppm	Nd ppm	$^{147}Sm/^{144}Nd$	$^{143}Nd/^{144}Nd$	2 SE	εNd (320 Ma)	T DM (Ma)	$^{87}Sr/^{86}Sr_i$ *
ASB 665	4.8	23.7	0.1224	0.512289	0.000006	−3.8	1358	
ASB 666	5.7	33.4	0.1032	0.512271	0.000014	−3.3	1158	0.7071
ASB 668	6.6	39.1	0.1020	0.512288	0.000008	−3.0	1124	
ASB 670	2.1	9.5	0.1336	0.512283	0.000008	−4.3	1546	0.7091
mean						**−3.6**	**1296**	**0.7081**
BER 788	5.5	29.5	0.1127	0.512293	0.000030	−3.3	1229	
BER 789	2.2	11.5	0.1156	0.512279	0.000003	−3.7	1284	
BER 790	0.7	2.1	0.2015	0.512421	0.000006	4.4	(6249)	
BER 791	2.3	11.9	0.1168	0.512279	0.000003	−3.7	1299	
mean						**−3.8**	**1271**	
KIB 786	4.2	20.2	0.1257	0.512319	0.000004	−3.3	1357	
KIB 794	6.5	32.2	0.1220	0.512308	0.000009	−3.4	1323	0.7064
KIB 796	7.3	37.0	0.1193	0.512269	0.000006	−4.0	1347	0.7076
mean						**−3.6**	**1342**	**0.7070**
EIB 612	0.7	2.2	0.1895	0.512466	0.000004	−3.1	(3510)	(0.7198)
EIB 712	1.8	6.9	0.1577	0.512334	0.000004	−4.3	2024	
EIB 718	4.1	18.2	0.1362	0.512223	0.000003	−5.6	1704	0.7090
EIB 719	4.2	17.4	0.1459	0.512278	0.000003	−5.0	1815	0.7104
mean						**4.5**	**1848**	**0.7097**

* according to [18], DM according to [49].

4.2. Zircon Geochemistry

Oxygen and Hf isotope ratios are given in the Table S2. The Hf and O isotope values are very similar for all samples and vary in a limited range (epsilon Hf from −3.9 to +2.4; Hf model ages (calculated according [57]) mainly between 1.3–1.2 Ga; $\delta^{18}O$ mainly between 6.0–9.0‰; with slightly higher scatter for EIB, especially for zircons/zircon rims with black CL). Zircon trace element data for two selected samples from EIB are presented in Table 3 (EIB 612, EIB 719).

Table 3. Trace elements in zircons. Temperature was calculated according to [58].

Spot	CL Pattern	Ca	Ti	Sr	Y	Nb	Ba	La	Ce	Pr	Nd	Sm	Eu	Gd	Dy	Er	Yb	Lu	Hf	Th	U	T (°C) [58]
sample EIB 612 (greisen)																						
1a		57.1	23.5	0.9	1418	18.5	2.4	0.4	25.2	1.1	8.6	10.2	0.3	35.2	131	242	419	65.3	8806	196	363	822
1b	black	8929	561	312	25,831	2604	3836	89.6	2875	327	2057	1654	84.4	2278	4116	2618	4579	610	17,864	21,134	25,298	1285
2a		59.4	15.0	1.4	2302	14.2	3.7	0.5	14.6	1.2	11.1	16.8	0.6	56.6	219	386	661	99.1	8950	231	1134	778
2b	black, porous	310	7.9	11.6	2045	27.4	64.7	2.9	31.1	5.4	38.0	46.3	3.0	86.3	241	275	822	125	25,610	121	6387	721
4a		14.5	15.3	0.7	2001	7.1	1.2	0.1	12.4	0.2	3.4	9.7	0.3	44.1	182	328	514	77.8	9658	233	501	780
4b	bright + black	95.6	15.2	1.2	2220	8.5	4.0	1.2	16.9	1.7	13.9	16.0	0.5	52.0	197	372	614	92.1	9197	265	812	779
5a		170	6.8	5.6	940	77.2	69.6	3.5	55.7	7.1	39.7	24.0	1.2	43.7	106	134	313	48.7	13,185	385	1487	708
5b	black + porous	4772	104	143	11,769	784	1214	137	2467	317	1759	925	39.8	1188	1699	1120	2413	341	23,168	2272	14,625	1000
6a		208	16.6	2.7	2292	49.5	38.1	5.1	180.4	15.9	92.1	51.2	3.0	98.9	237	359	625	97.8	7010	1416	1909	787
6b	black + porous	2175	40.6	32.9	6610	230	499	58.7	985.2	135	715	330	16.2	510	848	836	1387	205	7605	5419	6437	881
9a		6.3	22.8	0.5	1150	6.8	0.8	0.1	7.4	0.2	3.0	6.4	0.2	27.8	101	195	324	52.3	8093	99	181	819
9b	black	6026	127	226	12,463	528	1482	69.1	1566	226	1342	780	34.6	971	1522	1425	2783	376	15,856	2402	18,410	1027
12a		63.2	13.0	2.1	3309	22.2	6.2	0.6	31.6	3.0	24.5	25.8	0.9	77.5	291	518	833	127	9523	605	785	765
12b		17.1	8.7	0.9	1575	7.3	1.4	0.3	6.9	0.7	5.3	6.5	0.2	21.5	126	259	475	74.5	11,457	64	817	729
19a		32.4	9.7	1.3	3925	10.8	5.4	1.4	54.6	4.4	32.9	28.7	0.7	108	373	671	1011	150	7064	873	1041	738
19b	black	2765	16.3	18.7	9287	77.8	139.7	59.3	1953	238	1546	835	28.8	932	1218	938	1282	177	17,104	563	15,227	786
20a		16.8	19.9	1.6	1547	14.7	1.8	0.1	5.9	0.3	3.9	9.6	0.3	37.7	141	265	450	70.2	8494	183	332	806
20b	black + porous	12,689	565	684	32,604	4771	5935	108	1121	173	964	1414	92.9	2585	4739	2979	5641	700	29,834	1939	29,362	1286
21a		59.9	24.9	1.6	3608	44.0	6.9	0.8	43.4	3.6	36.0	38.3	1.5	116	341	582	896	137	8852	386	777	828
21b	black	3675	12.8	43.3	12,107	133	213	26.8	2346	174	1307	976	50.5	1373	1976	1167	1729	262	18,430	1383	14,542	763
sample EIB 719																						
B2		3.7	20.0	0.9	2385	14.2	1.2	0.1	6.5	0.3	5.1	11.2	0.4	56.0	211	411	658	103	8861	187	466	806
B3		19.8	21.4	1.0	2233	18.7	1.8	0.4	9.9	0.6	9.1	15.5	0.6	66.6	216	380	585	89.0	7984	240	405	812
B6		1854	12.7	2.8	2903	13.2	1.2	14.4	45.7	6.0	34.7	18.5	0.3	59.0	243	519	901	141	9389	150	721	762
B7		2.4	19.8	0.8	1512	13.7	0.7	0.1	6.1	0.1	2.8	7.2	0.2	33.6	133	263	447	69.8	8541	116	255	805
B8a		19.3	11.2	1.2	4606	14.9	1.5	2.6	41.4	2.0	20.2	30.5	1.0	126	429	750	1083	163	7302	941	1397	751
B8b	black CL	23.9	3.0	1.6	4998	11.5	1.4	0.3	1.3	0.1	1.1	5.9	0.1	48.6	407	706	1090	146	12,728	160	7957	644
A2		5.1	30.0	0.8	2693	32.4	1.2	0.2	31.6	1.0	14.0	20.2	5.6	84.5	258	448	733	114	7183	507	637	848
A5		1.1	27.9	0.8	2199	21.8	1.2	0.2	27.2	0.9	12.0	16.5	4.3	67.0	207	358	591	93.8	7102	394	499	840
A6		13.1	7.9	1.2	3100	16.5	1.0	0.2	4.5	0.2	2.2	6.9	0.2	43.0	260	492	803	117	10,628	133	1516	721
A8		6.9	24.0	0.8	2017	15.4	0.9	0.2	7.3	0.3	5.1	10.3	0.2	50.1	187	345	560	88.8	8616	147	279	824

5. Discussion

5.1. Identification of Source Rocks

The identification of source rock/s for highly evolved granites (that might be additionally overprinted by hydrothermal fluids) is a challenging task. Bulk rock geochemistry, as well as zircons (isotope composition and chemistry), have been used to infer on possible source/s. Here we use zircon for this discussion because it is an early crystallizing mineral in S-type granites and very robust against late-stage (e.g., hydrothermal) overprints. In contrast to bulk rock chemistry, $^{176}Hf/^{177}Hf$ isotope ratios in zircons are not affected by fractionation processes and hence represent the melt composition [59]. Melt production always results in increased Hf-isotope compositions in newly formed zircons compared to the source [59]. For our samples, all Hf isotope analyses show a remarkable homogeneity in their epsilon values (Table S2, Figure 3: most values between −3 to 0; zircons from EIB show a slightly larger scatter). This is in stark contrast to all sedimentary rocks from the Cadomian basement of Saxothuringia [60], and specifically to basement rocks from the Erzgebirge (Figure 3). Complete homogenization of zircons' Hf isotope ratios requires high degree melting and complete dissolution of former zircon grains [61]. This is rarely achieved in low-temperature (700–800 °C) S-type peraluminous granites that usually do not reach zircon saturation temperatures and, therefore, typically have abundant inherited zircons [55,61]. Based on the $^{176}Hf/^{177}Hf$ and $^{176}Lu/^{177}Hf$ data, meta-greywackes from the Cadomian basement (showing a large spread in Hf isotope composition) can be excluded as potential source rocks for the Variscan granites from the Western Erzgebirge (Figure 3).

Granitic zircons have very low Lu-Hf ratios (<0.001), often lower than common pre-Devonian basement rocks but similar to metamorphic zircons in amphibolite- and granulite-facies low degree melts (Figure 3, [17]). In addition, the Hf model ages from all granitic zircons are very homogeneous (1.3–1.2 Ga). Again, this is quite different to Cadomian basement rocks from the Erzgebirge [17]: grey meta-sedimentary Neo-Proterozoic gneisses: 3.7–1.0 Ga; red Ordovician gneisses: 1.6–1.0 Ga) and in general for Neo-Proterozoic-Cambrian basement rocks of Saxothuringia [60]: Late Neoproterozoic greywackes and quartzites: 4.3–0.8 Ga; Early Cambrian granites: 1.5–1.0 Ga). The newly formed high uranium zircons/zircon rims in granulite-facies melts have similar homogeneous model ages (1.3–1.2 Ga) but lower εHf values (from −7 to −4, [17]). Comparatively, zircons from metamorphic small scale melts in amphibolite-facies red gneisses yielded a slightly larger scatter (most model ages between 1.3–1.0 Ga but several cores with 1.5–1.9 Ga; εHf mostly between −6 and 0, and a few cores with values from −19 to −11 [17]). In general, all four granite suites display a very similar pattern in the Hf-O-isotope diagram (Figure 4). The relatively low and homogeneous $\delta^{18}O$ values (mainly within 6.0–8.5‰) exclude sediments (e.g., shales) as main source rocks that display typical values ≥14‰ (specifically, Ordovician shales have typical $\delta^{18}O$ values between 12 and 20‰; [62]).

The CaO/Na_2O ratio of bulk rocks was used to infer source rock composition [56]: low CaO/Na_2O ratios (<0.3) indicate pelitic (plagioclase free) sources but not greywackes (CaO/Na_2O = 0.3–1.5) or meta-igneous rocks (CaO/Na_2O = 0.3–1.5). Almost all of our samples have low CaO/Na_2O ratios (≤0.3; Table 2). In addition to pelites and shales, garnet- and muscovite bearing restites left behind after granulite-facies melting have low CaO/Na_2O ratios (<0.47) because they are poor in plagioclase, but have high Al_2O_3 (15–20 wt%) and K_2O contents (4.5–5.0 wt%; [17]). These rocks correspond to assemblage 3a according to Willner et al. [11] and are one of the three most common peak PT assemblages of (U)HP gneisses from the central Erzgebirge [11,63]. Among these gneisses, they recorded the highest water activities at maximum PT conditions [11]. In addition, they experienced retrograde recrystallization of kyanite to muscovite that was probably accompanied by fluid flow [11,63]. Therefore, its unusual chemical composition (low Ca, high K, [11,63]) can partly be explained by the high water activity at maximum PT and fluid overprint at the retrograde metamorphic path (P = 1.5–1.8 GPa, T = 750 °C; [63]). Therefore, also from the low CaO/Na_2O ratios, these rocks fit as a feasible and fertile source for the Variscan granites.

Compared to typical S-type granites, xenocrystic zircon ages are remarkably scarce in the investigated samples (<5%). Figure 5 shows a compilation of published xenocrystic ages from various zircon dating methods (data from [18,64]). The largest age peak corresponds to 360–340 Ma pointing to metamorphic rocks as the main protoliths for these Variscan granites (Figure 5).

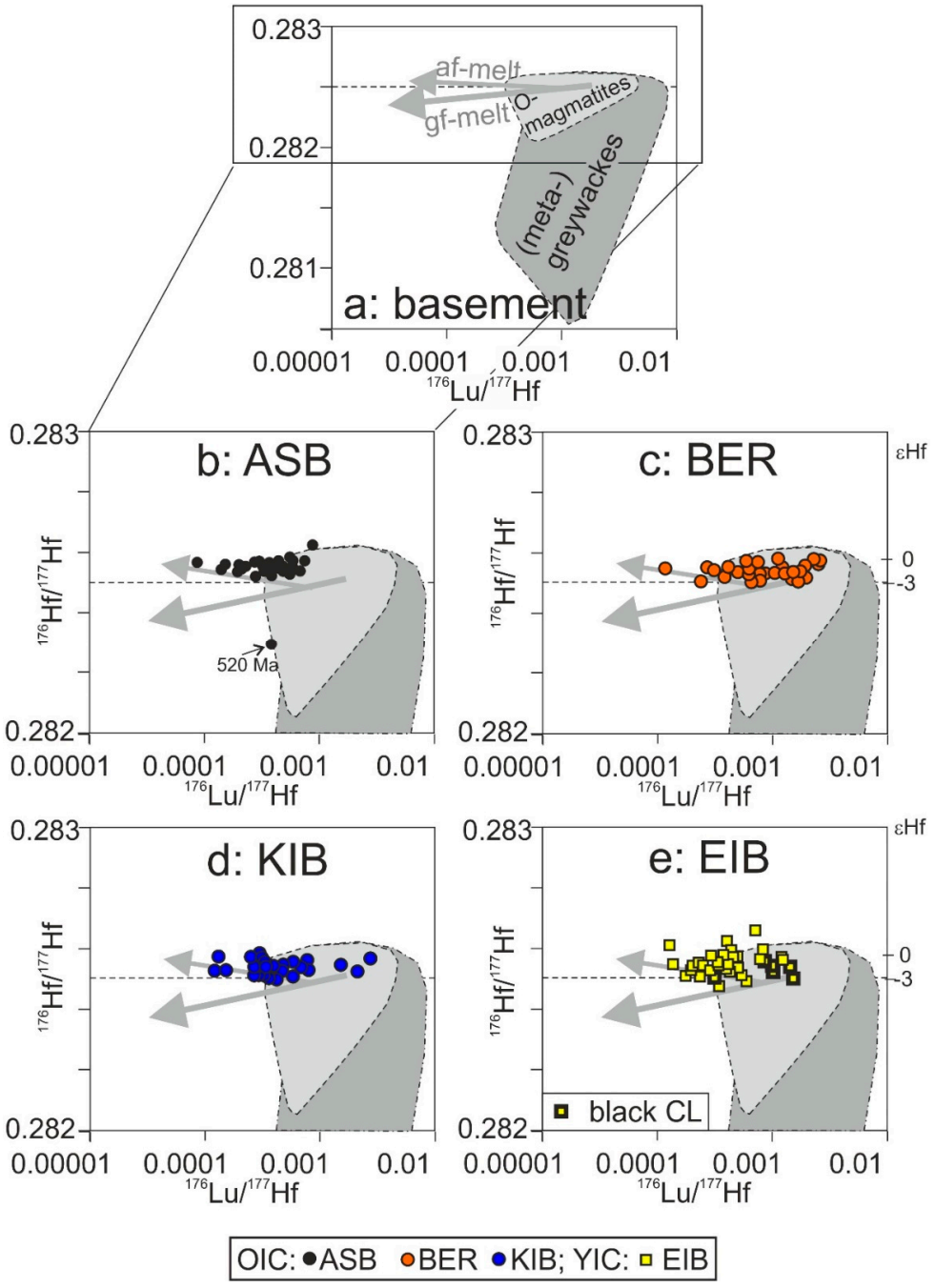

Figure 3. $^{176}Lu/^{177}Hf$ ratios versus $^{176}Hf/^{177}Hf$ ratios from the same spot locations of zircons from Variscan granites. (**a**) typical variation of potential host rocks [17], also shown in comparison to ASB (**b**), BER (**c**), KIB (**d**), and EIB (**e**): Neoproterozoic grey gneisses (meta-greywackes), Ordovician red orthogneisses (O-magmatites,) amphibolite-facies melts (af-melts), and granulite-facies melts (gf-melt; data from [17]). Measurements for zircons having black CL images are shown with a thick black rim of the corresponding sign. OIC—older intrusive complex, YIC—younger intrusive complex. The dashed line corresponds to a $^{176}Hf/^{177}Hf$ value of 0.2825 and is shown for better comparison.

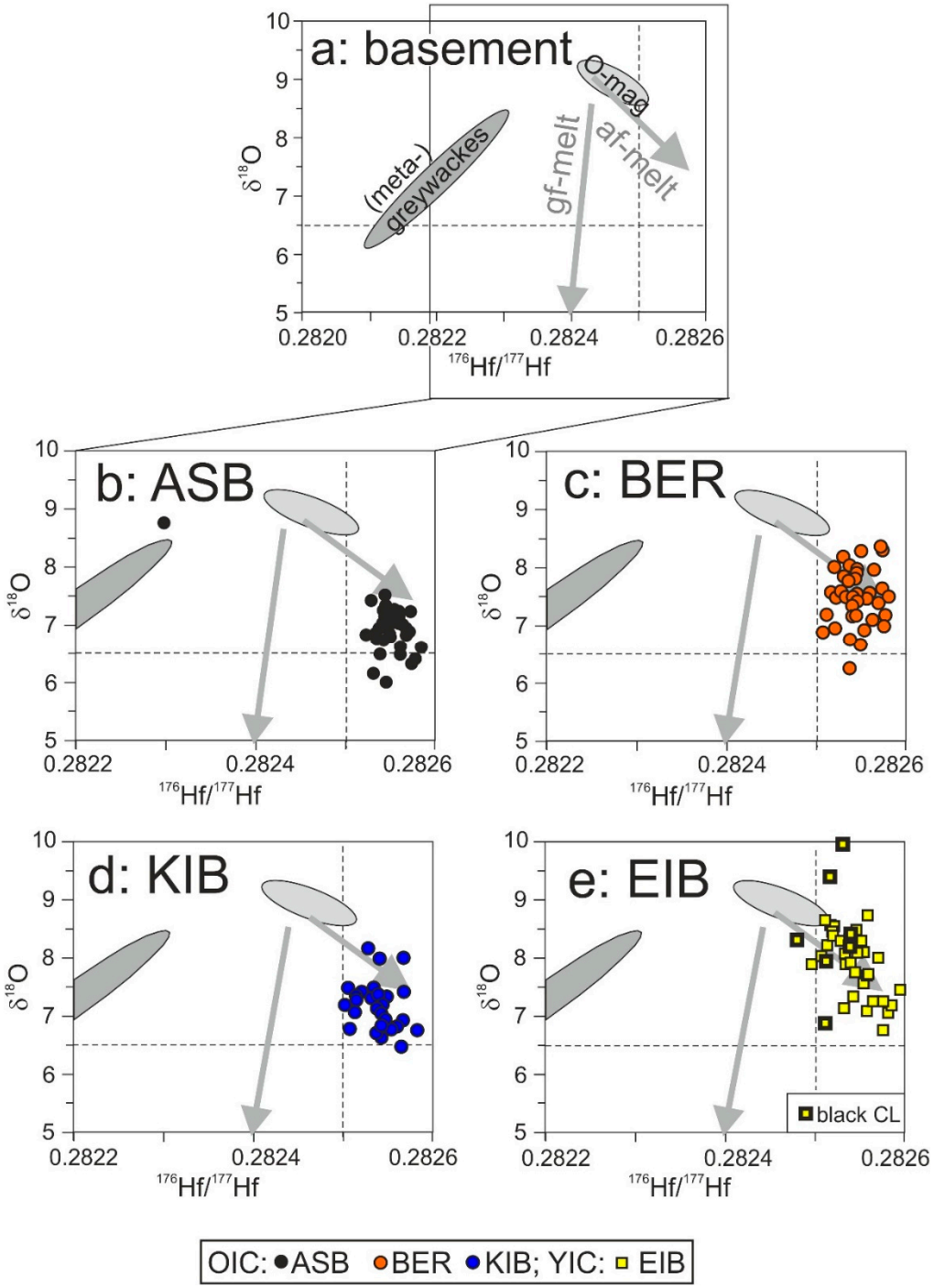

Figure 4. $^{176}Hf/^{177}Hf$ ratios versus $\delta^{18}O$ values from the same spot locations of zircons from Variscan granites. (**a**) typical variation of potential host rocks, also shown in comparison to ASB (**b**), BER (**c**), KIB (**d**), and EIB (**e**): Neoproterozoic grey gneisses (meta-greywackes), Ordovician red orthogneisses (O-magmatites,) amphibolite-facies melts (af-melts), and granulite-facies melts (gf-melt; data from [17]). Measurements for zircons having black CL images are shown with a thick black rim of the corresponding sign. OIC—older intrusive complex, YIC—younger intrusive complex. The dashed lines correspond to a $^{176}Hf/^{177}Hf$ value of 0.2825 and to a $\delta^{18}O$ value of 6.5‰ and are shown for better comparison.

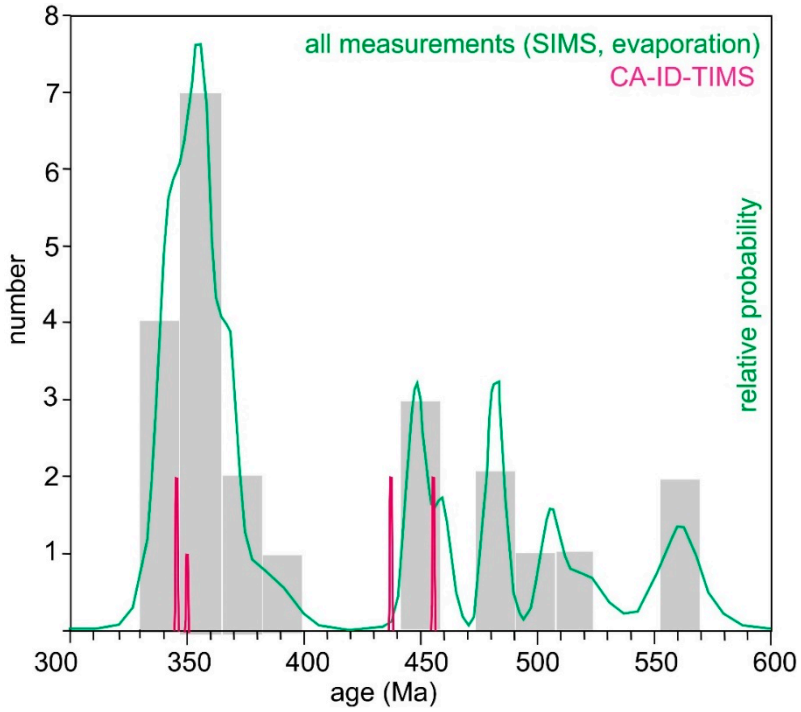

Figure 5. Compilation of xenocrystic ages (n = 23 from a database of ~520 measurements, [18,64]) from all analyzed samples from ASB, BER, KIB, and EIB.

Bulk rock Nd model ages from ASB, BER, and KIB vary from 1.3–1.1 Ga and are consistent with Hf model ages from zircons (except one sample where Nd concentrations are <10 ppm and consequently $^{147}Sm/^{144}Nd$ ratios are >0.15; sample BER 790; Table 2). These Nd model ages are considerably younger than those of Cadomian basement rocks from Saxothuringia while their εNd values are slightly higher (Figure 6; [8,14,65]: grey gneisses = 1.8–1.6 Ga, Ordovician red gneisses: 1.6–1.5 Ga). No Nd isotope data were published for Paleozoic sedimentary rocks (shales, arkoses) from Saxothuringia. Cambro-Ordovician shales and pelites from other regions of the Variscan belt (Iberia, French Massif Central) have typical Nd model ages between 1.8 and 1.4 Ga [66–68] that are distinctly older compared to analyzed granites. Unfortunately, no Nd model ages were published for zircons from granulite-facies rock in the Erzgebirge, but their Hf model ages are 1.3–1.2 Ga (see discussion above). Samples from EIB show a tendency towards higher Nd model ages. At least for the greisen sample (EIB 612), the high model age resulted from very low Nd concentrations and related high $^{147}Sm/^{144}Nd$ ratios that could be caused by the strong hydrothermal overprint.

Collectively, Hf and O isotope data from zircons, scarce xenocrystic zircon ages as well as Nd bulk rock model ages record a source that is more homogenized than all known low-grade metamorphic Cadomian basement rocks from Saxothuringia. Consequently, pure sediments and most meta-sedimentary and meta-igneous host rocks from the Cadomian basement can be excluded as major sources. Contrary, high-grade metamorphic amphibolite- and granulite-facies gneisses are the most likely sources for Variscan granites in the Western Erzgebirge based on their zircon data (Hf and O isotopes, xenocrystic ages). The Hf data from zircons as well as the Nd data from whole rocks do not support a substantial mantle input for these S-type granites after metamorphic homogenization.

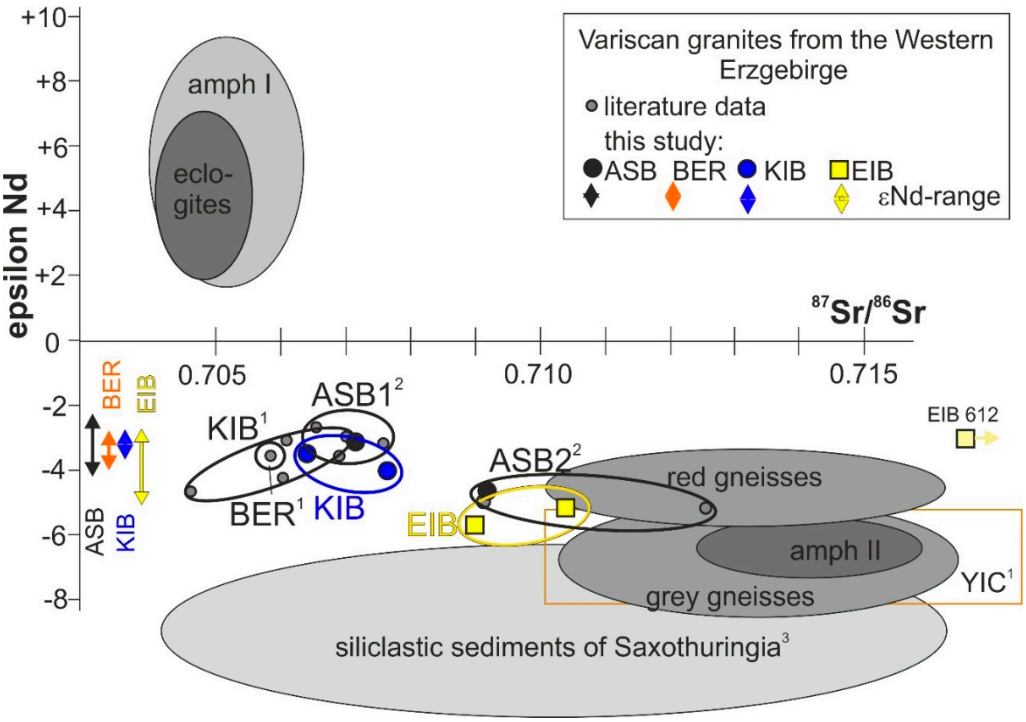

Figure 6. $^{87}Sr/^{86}Sr_i$ versus epsilon Nd for bulk rocks. Literature data for granites: [1]—[4], [2]—[5]. ASB1 corresponds to samples from the Aue subgroup (northern biotite granites), ASB2 to samples from the Schwarzenberg subgroup (southern two-mica granites). Variations of basement host rocks from the Erzgebirge and Saxothuringia are shown as grey fields. Data from: [3]—[36] for siliclastic sediments of Saxothuringia, [23]: eclogites, amphibolites I (amph I), amphibolites II (amph II), red and grey gneisses.

5.2. Fractional Crystallization and Mixing

Granites often show large and correlated variations in element concentrations. Most authors interpret such trends as fractional crystallization, e.g., [2,4,69,70]. The combined decrease of MgO, TiO_2, and CaO (compare Section 4.1) indicates a correlated fractionation of biotite and plagioclase that explains the trend in Figure 2c. In addition, element concentrations vary depending on their structure: samples with large K-feldspar phenoycrysts (that can make up ~15% of rocks) plot at the undifferentiated end (lower SiO_2 contents) while fine-grained varieties without phenocrysts plot at the opposite "fractionated" end of such trend lines (Figure 2). Trend lines imply K-feldspar loss due to fractional crystallization (in addition to the combined fractionation of biotite and plagioclase) in the fine-grained evolved granites (Figure 2c). Alternatively, variations in element concentrations can be explained by mixing. We prefer the interpretation of [40] where phenocrysts comprise early crystallization products and the fine- to medium-grained matrix represents the late-stage crystallized melt. Then, this mixing is responsible for the correlated variations in element concentrations (Figure 2). Accordingly, [71] used the term "phenocryst unmixing" and demonstrated that this process results in linear trends on Harker diagrams.

The Ti content of bulk rocks was often used as an indicator for fractional crystallization, e.g., [4]: lower Ti concentrations correspond to higher degrees of fractionation. On the other hand, Ti was used as a temperature indicator, e.g., [56]: using Al_2O_3/TiO_2). Strong positive inter-correlations between Ti, Zr, and Si were shown to be typical for all S-type granites [72,73]. In addition, Ba is strongly positively correlated with Zr in S-type granites (compare the good correlation of Ba with TiO_2 in Figure 2b, but Ba correlates also with SiO_2, Zr, Rb, and Sr in our samples–not shown). In contrast, most I-type granites show a random scatter between Ba and Zr contents [73]. During melting Ba partitions into melt as biotite and feldspars break down. In [73], higher Ba concentrations from a given source were explained as resulting from a higher melting degree (corresponding to higher melting temperatures)

and different slopes in Ba-Zr diagrams for various granite plutons as reflecting diverging Ba contents in their sources. Accordingly, coarse-grained porphyritic granitic varieties from ASB and KIB would indicate the highest melt degrees and melting temperatures for our samples (Figure 2d).

Several approaches exist to calculate melt temperatures. The granite samples from KIB show a good correlation between the Ba content and the calculated zircon saturation temperature (Figure 2d). They record a temperature variation of ~80 °C (830–750 °C) within the KIB pluton. A similar relationship is displayed by all porphyritic varieties from ASB while their fine-grained rock types without K-feldspar phenocrysts do not show a correlation of Ba contents with zircon saturation temperatures (Figure 2d). There is no inter-correlation between Ba contents and calculated zircon saturation temperatures for EIB samples (Figure 2d). Figure 7 compares melt temperatures obtained from various approaches. Accordingly, KIB granites tend to the highest temperatures followed by ASB. The latest intrusion (EIB) yielded similar or even lower temperatures compared to earlier plutons (ASB, BER, KIB).

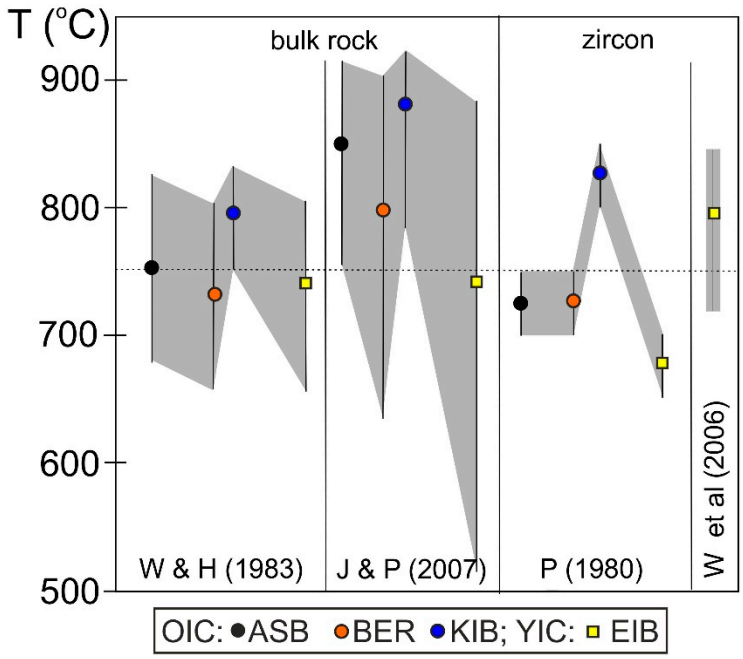

Figure 7. Calculated melt temperatures and their variations. Plutons have been arranged according to their intrusion sequence. Watson and Harrison (1983)—Zircon saturation temperatures according to [55]. Note that temperatures calculated according to [74] will be c. 50 °C higher. Jung and Pfänder (2007)—calculated according to [56]. Pupin (1980)—calculated according to [75] using zircon morphology (shown in [18]). Watson et al., (2006)—calculated according to [58] using Ti in zircon data from sample EIB 719 (activity was set to 1 for Ti.) Correction for lower Ti activity would result in higher temperatures [76]. OIC—Older intrusive complex, YIC—younger intrusive complex.

Summarizing, we interpret the observed element correlations, at least for the early intrusions (OIC: ASB, BER, KIB: SiO_2 correlates negatively with MgO, Al_2O_3, TiO_2, and CaO, V, Zr, Ba—described also in previous publications), mainly as the result of "phenocryst unmixing" (Kfs, Plg, Bt) that may be also related to melt temperatures (porphyritic varieties may have higher melting degrees and melting temperatures).

In contrast to elements, isotope ratios (of the same element) are not affected by fractional crystallization and should sensitively unravel the mixing of different sources. We stated earlier that both Hf and O isotope ratios of zircons are more homogeneous than most pre-Devonian basement rocks (Section 5.1). However, there are subtle differences between plutons: ASB and KIB have the lowest mean $\delta^{18}O$ values followed by BER and then by EIB (Figure 8a). The corresponding whole- rocks (calculated according to [77]) display $\delta^{18}O$ values between 8.5–9.0‰ for ASB and KIB, 9.0–9.5‰ for

BER, and 9.5–10.0‰ for EIB (Figure 8b), indicating a slightly higher input of crustal (sedimentary?) sources for the later intrusions (BER, EIB). Using the classical definition for I- and S-type granites [78] both the $\delta^{18}O$ values and the $^{87}Sr/^{86}Sr_i$ ratios indicate rather an I-type or an intermediate I/S-type source for KIB and for the northern part of ASB (ASB1 in Figure 6). The higher crustal influence for BER and EIB, however, is not adequately recorded by lower Nd isotopes and Hf isotopes. Only for EIB samples, higher Sr isotope ratios are in line with the highest $\delta^{18}O$ values of zircons. In addition to the described differences in $\delta^{18}O$ values between plutons, KIB samples have lower epsilon Hf values compared to those from ASB (Figure 8a). All these differences in isotope ratios indicate diversities in the protoliths between the four plutons but also between samples from the same pluton. The three samples from KIB define a trend line from porphyritic to fine-grained granites with increasing mean $\delta^{18}O$ values that might be interpreted as an evolution line (Figure 8b). However, samples from ASB, BER, and EIB do not display such trends. Note, that all samples display large within-sample-variations both for epsilon Hf and $\delta^{18}O$ values (Figure 8a) that should also indicate some changes in sources or mixing processes.

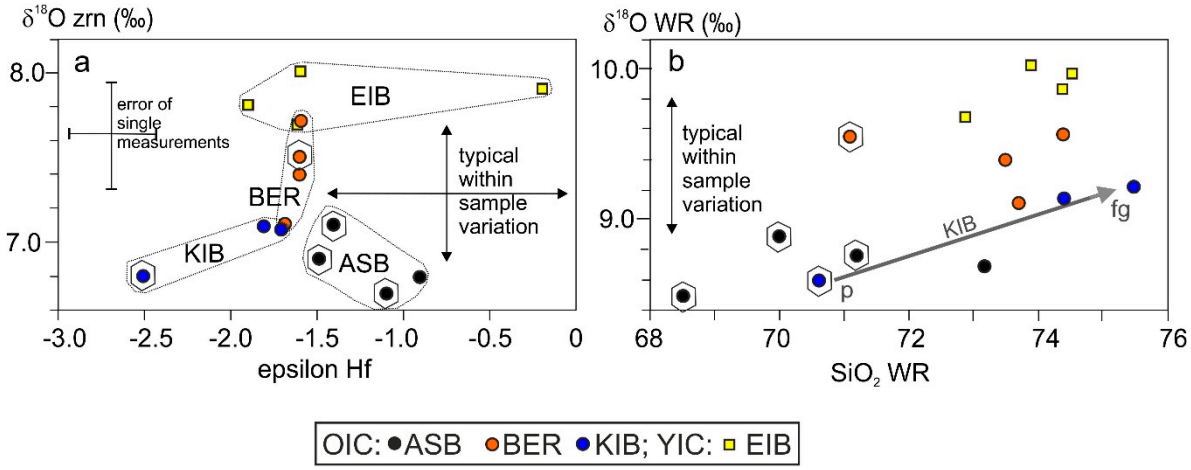

Figure 8. (**a**) Mean epsilon Hf versus mean $\delta^{18}O$ values from zircons for each sample. In addition, the range of typical within sample variations of measurements for a single sample is shown. (**b**) SiO_2 concentrations from whole rocks (as an indicator of differentiation, compare Figure 2) versus $\delta^{18}O$ of whole rocks calculated from $\delta^{18}O$ values of zircons according to [77]. p—porphyritic, fg—fine-grained; OIC—older intrusive complex, YIC—younger intrusive complex.

5.3. Effect of Greisenization on Geochemistry

5.3.1. Bulk Rock Geochemistry

Different greisenization types have been described in the Erzgebirge/Krušné Hory that enriched several elements to various degrees (e.g., [3,28]: Sn, W, Ta, Nb, F, Bi). Greisen formation has been related to various processes like late magmatic, post-magmatic, or hydrothermal element mobilization, e.g., [3,28].

We analyzed two greisen samples from the EIB pluton (EIB 612, EIB 713). The thin section of sample EIB 612 was investigated in detail by optical microscopy combined with cathodoluminescence [18]. Figure 14 in [18] showed typical replacement textures of this greisen sample: all feldspars were replaced by a fine-grained intergrowth of fluorite, Li-mica, cassiterite, and apatite.

Both greisen samples have considerably lower Na_2O contents compared to hosting granite samples (0.1–0.2 wt% compared to 2–3 wt%), while the SiO_2 content is higher only for one sample (EIB 713: ~83 wt%). In addition, both samples have relatively high contents of F, Rb, Cs and low contents of Ba, Sr, TiO_2, LREE that are comparable to some of the highly evolved fine-grained EIB granite samples. However, there is a clear enrichment in Sn (137 and 505 ppm compared to ≤42 ppm), W (29 and 49 ppm compared to ≤14 ppm), and Bi (1060 and 46 ppm compared to ≤17 ppm) compared to all other

non-greisenized EIB samples. The observed changes (replacement textures with a formation of fluorite, geochemical enrichment/depletion) can best be explained by post-magmatic or hydrothermal element mobilization by a F-rich fluid that was able to enrich distinct ore elements (Sn, W, Bi) by a factor of ≥2–62.

5.3.2. Zircon Geochemistry

We measured trace elements within zircon grains from two samples from Eibenstock: the porphyritic sample EIB 719 and the greisen sample EIB 612 (Table 3). Zircons from the granite sample show typical oscillatory zoning in CL images [18] and typical REE pattern with positive Ce and negative Eu anomalies (Figure 9a). Many zircons from the greisen sample have thick black CL rims and inner core regions with oscillatory zoning (Figure 9b,c). The core regions show similar REE patterns compared to zircons from sample EIB 719 (Figure 9b) while the black CL zones are strongly enriched in LREE (Figure 9c). In addition, these rims are enriched in Ca, Sr, Ba, Y, Nb, Th, U, Hf and sometimes in Ti (leading then to too high calculated Ti-in-zircon temperatures; Table 3), and in common Pb [18]. Therefore, the greisenization led to considerable changes in the chemistry of black CL zircon rims, while the inner core regions preserved most primary magmatic information. Elements in CL black rims are often at least 10 times enriched but can reach enrichment factors of ~700 compared to CL zoned cores from the same zircon grain (Table 3) and require extremely high degrees of element mobilization. Such high enrichment factors cannot be achieved by a fractionated new melt batch but indicate an F-rich fluid that was able to dissolve high concentrations of chemically different elements.

5.4. Factors Necessary for Enrichment of Sn and W to Ore Concentrations

In literature, several factors like source enrichment of granitic melts, their temporal evolution up to highly evolved granites, and enrichment processes in hydrothermal fluids are discussed as important factors to enrich Sn and W up to ore levels. In the following, we discuss the impact of these processes.

5.4.1. Source Enrichment

Homogenized granulite- and amphibolite-facies metamorphic rocks are the most likely sources for the granites (compare Section 5.1). According to [17], grey gneisses (specifically the Neo-Proterozoic (~575 Ma) meta-greywackes) are suggested as the precursors of granulite-facies rocks. In Figure 10, we compare the bulk rock composition of basement rocks including granulite-facies melts and their restites to look for Sn and W enrichment processes. The grey gneisses are only slightly enriched in Sn and W (by a factor of 2) compared to the upper continental crust (UCC). Ordovician red gneisses display some higher enrichment (by a factor of 3–4) where some single rocks may have Sn enrichments of 6–9 times compared to UCC. Restite layers left behind after granulite-facies melting consists mainly of muscovite, quartz, and garnet and show the highest mean enrichment for Sn (by a factor of 6–7) with less enrichment for W (~3 times UCC). Layered granulitic gneisses are quite common in the central Erzgebirge especially in the (U)HP region [11,63]. The abundant muscovite crystals were formed at the retrograde path replacing kyanite (P = 1.5–1.8 GPa, T = 750 °C; [63]). The formation of muscovite took place at high water activities [11,63] and could lead to the enrichment of some incompatible elements in the mica. The metamorphic muscovite was dated by Ar-Ar yielding ~340–330 Ma [79]. Restite layers were interpreted as resulting from multiple melt extractions [17]. Although the melanocratic restite layers have Zr concentrations comparable to melt layers only tiny resorbed zircons could be found that often were enclosed in large garnet grains [17]. However, the restite layers contain abundant Fe-Ti-minerals (mainly rutile and ilmenite) along with large monazite grains [17]. Rutile from the (U)HP region of the Erzgebirge often contains extremely high Zr concentrations because of its high formation temperatures (~1000 °C; [80]). It has been repeatedly shown that various Fe-Ti-minerals (e.g., rutile, ilmenite, titanite) can contain very high concentrations of Sn ([81]: up to 15% in titanite; [82]: up to 1.7%; [83]: up to 600 ppm in rutile), and W ([82]: up to 9% in rutile; [83]: up to 1200 ppm in rutile). High Zr concentrations in rutile often correlate with high concentrations of other elements, e.g., Sn and

W [83]. Therefore, we propose that rutile could concentrate both Sn and W due to the high temperature during (U)HP metamorphism that led to high enrichment of both elements in the restites (having higher abundances of rutile compared to melt rich layers). In addition, muscovite and garnet of the restite could be enriched as these minerals also can incorporate Sn and W to various degrees [84–86]. In summary, the source rocks were already enriched in Sn and W, but less than 10 times compared to UCC.

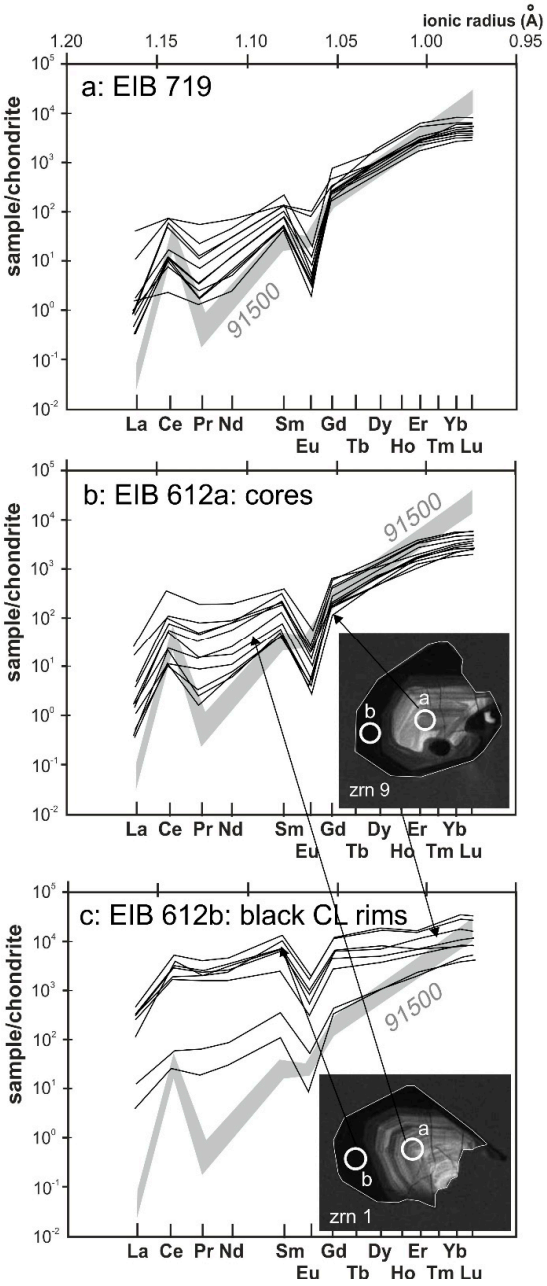

Figure 9. Chondrite normalized (according to [87]) REE pattern of spot measurements within zircon grains from two Eibenstock samples. (**a**) on CL oscillatory zoned zircons from the porphyritic sample EIB 719, (**b**) on CL oscillatory zoned zircon cores from the greisen sample EIB 612, (**c**) on dark CL zircon rims from the greisen sample EIB 612. In (b) and (c) examples of CL images for two zircon grains from EIB 612 and their spot locations are shown.

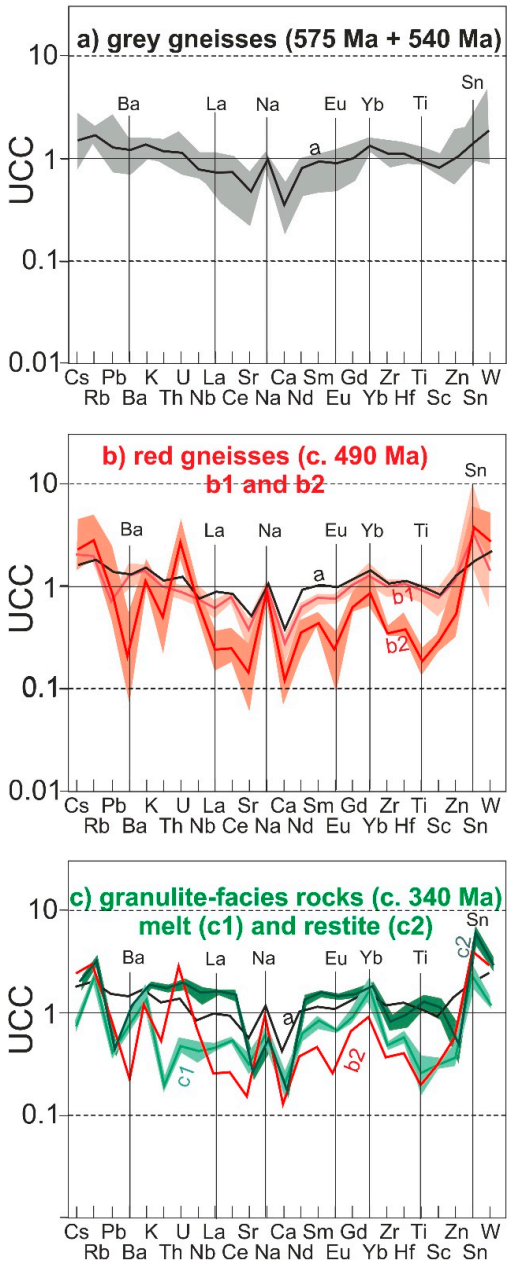

Figure 10. Geochemical signatures (spidergrams) of basement rocks normalized to the average concentration of the upper continental crust (UCC) after [88]. Diagrams show mean values and their typical variations. (**a**) grey gneisses represent Neo-Proterozoic meta-greywackes (~575 Ma) and Cambrian (~540 Ma) orthogneisses. Both rock types have very similar bulk rock geochemistry. Data are from [16]. (**b**) red gneisses represent unfractionated (**b1**) and highly fractionated (**b2**) Ordovician (500–480 Ma) orthogneisses. Data are from [16]. (**c**) granulite-facies melts (**c1**) and restites (**c2**). Data are from [17].

5.4.2. Enrichment During the Geochemical Evolution of Variscan Granites

For all granites from the OIC, Rb concentrations increase from porphyritic to more fractionated fine-grained melt enriched varieties. Together with Rb concentrations, also the Sn and W concentrations increase in OIC (Figure 11e,f). Accordingly, the mean enrichment factor increased during the evolution of OIC melts from a factor of 3 to about 12 for Sn, and from about 1 to 7 for W compared to UCC (some of the BER samples yielding the highest enrichments). The EIB granites intruded about 5 Ma later than the latest OIC intrusions [18]. All samples from EIB are enriched in Sn (by a mean factor of 12)

and W (by a mean factor of 7 compared to UCC; some samples from BER show a similar enrichment; Figure 11e,f). Therefore, multiple melt production in the crust over a time span of about 9 Ma (from 323 to 314 Ma) lead to a substantial overall enrichment of Sn and W in the YIC (Figure 11a,b). For the EIB samples, increasing Rb concentrations (correlated with increasing F (Figure 11c) and Cs concentrations, slightly increasing Nb and Ta concentrations, and decreasing TiO_2, Ba, Sr and REE concentrations) do not correlate with W (Figure 11f), i.e., magmatic fractionation within the EIB granite did not lead to further enrichment of W. Sn concentrations of EIB samples, however, seem to weakly increase with Rb concentrations and reach overall enrichment of ~15 times of UCC with few exceptions enriched up to ~40 times (Figure 11e). In addition, a few samples are exceptionally enriched in W up to ~18 times of UCC (Figure 11f).

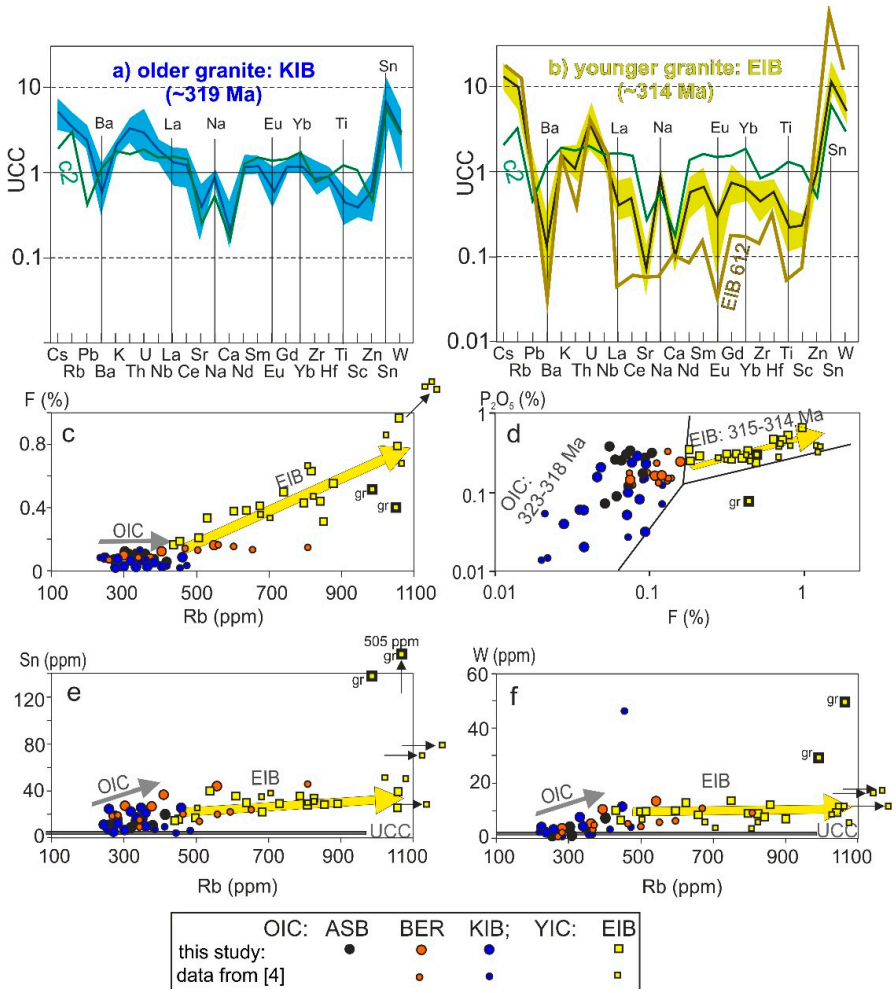

Figure 11. Geochemical signatures of Variscan granites. (**a**) spidergram of samples from the Kirchberg granite—as a representative for OIC—normalized to the average concentration of the upper continental crust (UCC) after [88]. For comparison, the mean curve for restites of granulite-facies melts (c2 from Figure 10c) is shown. (**b**) spidergram of samples from the Eibenstock granite—as representing YIC—normalized to the average concentration of the upper continental crust (UCC) after [88]. For comparison, the mean curve for restites of granulite-facies melts (c2 from Figure 10c) is shown. In addition, the line for the greisen sample (EIB 612) is presented. (**c**) Rb versus F concentrations. (**d**) F versus P_2O_5 concentrations - discrimination diagram after [4] with different fields for low-F OIC granites and high-F EIB granites. Position in this diagram can be taken as evidence if samples belong either to OIC or YIC in the Western Erzgebirge. (**e**) Rb versus Sn concentrations. Value for the upper continental crust (UCC) from [88] = 2.1 ppm. (**f**) Rb versus W concentrations. Value for the upper continental crust (UCC) from [88] = 1.9 ppm. OIC—older intrusive complex, gr—greisen.

5.4.3. The Role of Hydrothermal Processes for Enrichment

We analyzed only two greisen samples that represent a very restricted part of the whole variability of different greisen types in the Erzgebirge/Krušné Hory. One sample (EIB 612) was dated by both Rb-Sr and Ar-Ar methods yielding slightly different ages [18]. Nonetheless, from these dating results, the authors concluded that this greisen was formed either contemporaneous with magma intrusion or slightly later (8 Ma), but it belongs to the first period of magmatic activity [18]. Simple fluid unmixing directly from the melt would result in identical $^{87}Sr/^{86}Sr_i$ ratios of melt and unmixed fluid. The considerably higher $^{87}Sr/^{86}Sr_i$ ratio for the greisen sample EIB 612 (compared to other EIB samples) does not support a simple fluid-melt partitioning process. Therefore, we suggest a (slightly?) later hydrothermal process that led to greisenization. Both samples (EIB 612, EIB 713) clearly demonstrate that both Sn and W are highly enriched (Sn: 65 and 240 times, W: 15 and 26 times compared to UCC). Consequently, at least for this type of greisen, the hydrothermal processes are the most important step to ore level enrichment. Remarkably, the greisen samples have neither the highest F nor P concentrations (Figure 11c,d) although both elements may play an important role in the element mobilization processes. We suppose that the high enrichment in hydrothermal greisen fluids was possible due to a thick continental crust composed in large parts of Variscan granites (supported by several boreholes and the negative Bouguer anomaly; compare Section 2) that were already enriched in these elements.

In summary, there is an enrichment of both Sn and W with time in the source(s) of granitic melts, but the enrichment degree is relatively low (Figure 12). Our data do not support the suggestion that weathering related Sn and W enrichment of sedimentary rocks is an important control for granite hosted Sn (and W) ore formations [6]. The low $\delta^{18}O$ together with relatively high Hf isotope data on zircons from granites contradict assumptions on the important role of intensely weathered shales as the most important source rock for Variscan granites [6,7]. Low temperature weathering always results in high $\delta^{18}O$ values of such sediments with typical values >12‰ [62]. Specifically, $\delta^{18}O$ values range from 12 to 24‰ in Cambro-Ordovician shales [62]. Instead of intense weathering, low Ca and Na together with high K concentrations were reached in restites by melting under granulite-facies conditions and subsequent retrograde metamorphic fluid overprint (Figure 10). Differently to the Cornubian Variscan Batholith, we can exclude (meta-) greywackes as the main source rocks [2] because of the relatively homogeneous Hf isotope data and their model ages. However, (meta-) greywackes could be the protolith for (ultra-) high-pressure granulites where local melting resulted in resorption of former zircons and homogenization of their Hf values [17].

There is a further Sn and W enrichment due to multiple melt production in the older igneous Variscan complex (OIC) during 323–318 Ma, but this enrichment is usually not higher than 12 times the UCC level (Figures 11 and 12). Fractionation within EIB granites leads to additional overall Sn enrichment up ~15 times of UCC (Figure 11e), but for W this enrichment stays at ~7 times of UCC (Figure 11f). Therefore, we conclude that the role of fractional crystallization is very important but the enrichment degrees were often overestimated. The idea that multiple melt extraction at high-temperature results in strong Sn enrichment in late high-temperature melts [7] is not in line with our data where the latest melts (EIB) show a tendency towards lower temperatures. However, multiple melt productions were certainly important for a general Sn and W enrichment in the crust; the OIC and EIB granites document this process.

The largest Sn and W enrichment was achieved by hydrothermal fluids leading to greisen ore bodies (Figure 12). We agree that both the source composition and the Sn (and W) hosting mineral/s played an important role in their later mobilization [7]. In addition, the fluid composition determined what minerals were dissolved and what elements were transported. In the Western Erzgebirge, granites from the YIC are remarkably enriched in F (Figure 11d) and the formation of fluorite in the greisen sample documents a high fluorine activity in the greisen fluid.

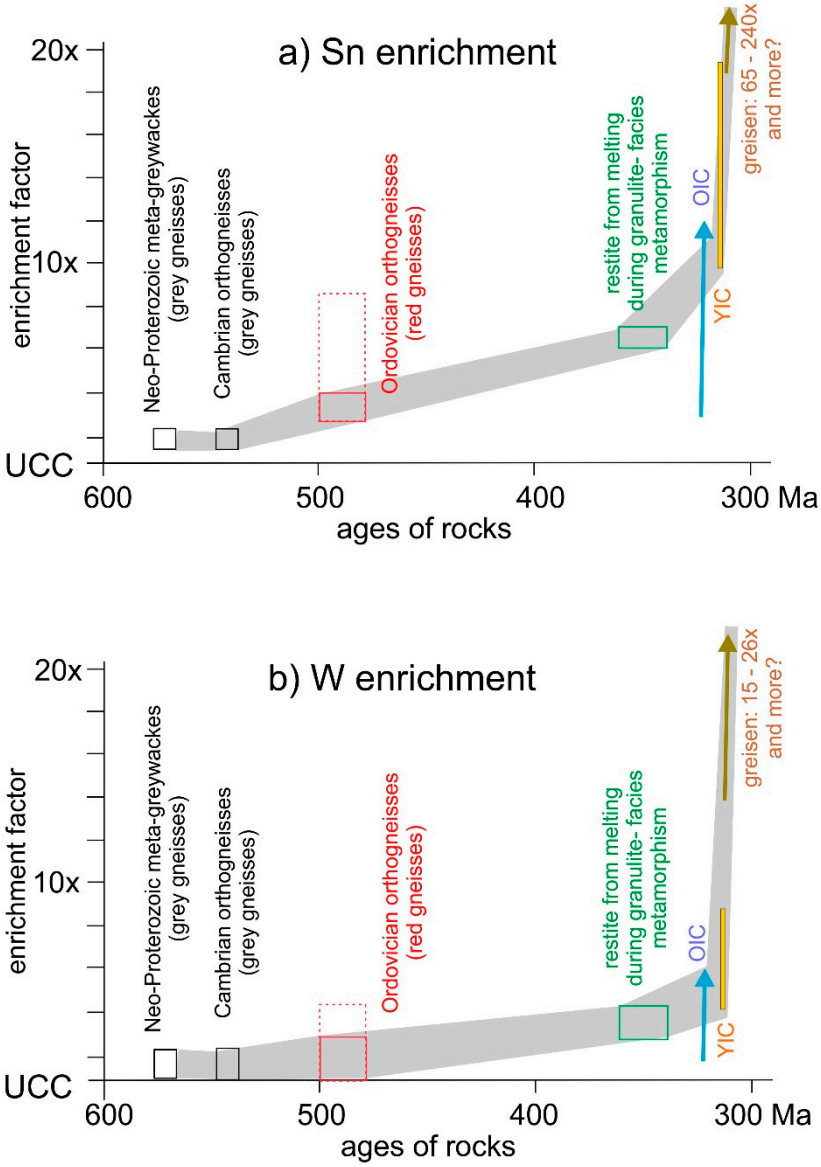

Figure 12. Sn enrichment (**a**) and W enrichment (**b**) in the crust of the Western Erzgebirge versus time. UCC after [88]. Stippled box for Ordovician orthogneisses corresponds to highly fractionated gneisses (compare b2 in Figure 10).

6. Conclusions

The most feasible source rocks for the Variscan granites from the Western Erzgebirge are high-grade metamorphic (amphibolite- and granulite-facies) rocks. This conclusion is based on Hf and O isotope composition of zircons, the abundance of xenocrystic ages, and Nd model ages.

We interpret the trend lines in Harker diagrams (bulk rock geochemistry) as fractional crystallization (of biotite and plagioclase) combined with K-feldspar phenocryst unmixing. Porphyritic varieties may correspond to higher melt temperatures. We calculated melt temperatures that vary up to 80–150 °C within each pluton. Calculated temperature ranges overlap, but KIB granites tend to higher temperatures while the latest EIB granites tend towards lower temperatures. Hf and O isotopes on zircon reveal only subtle differences in granitic sources: EIB granites record a slightly higher crustal input.

In contrast to previously published suggestions [6,7], we can exclude a substantial role of intense sedimentary weathering as an important control factor for later Sn and W enrichment in granite related ores of the Western Erzgebirge due to the remarkable homogeneous Hf and low O isotopes in granitic

zircons that are extremely distinct to all pre-Devonian basement rocks of Saxothuringia. We document a source enrichment from meta-sedimentary rocks (575 Ma) towards metamorphic rocks (340 Ma) were restites from granulite-facies melts are enriched 6–7 times in Sn compared to UCC. These rocks are also enriched in K, but depleted in Na and Ca, contain abundant muscovite, and are fertile for later melting. Further enrichment of Sn and W occurred during multiple melt production of the older igneous granites (323–318 Ma) leading finally to a general enrichment of Sn (15 times compared to UCC) in the tin granites. Multiple melt production did not lead to a very strong enrichment of ore metals in the granites but is probably very important for a general enrichment of Sn and W in the thick granite-rich crust of the Erzgebirge. Efficient leaching by hydrothermal fluids led to a very strong enrichment (up to several orders) of Sn and W in the greisen ore bodies.

Supplementary Materials: The following are available online at http://www.mdpi.com/2075-163X/9/12/769/s1, Table S1: Bulk Rock Geochemistry of Investigated Samples, Table S2: LA-MC-ICPMS Lu-Hf Data and SIMS Oxygen Data of Zircons.

Author Contributions: Conceptualization, M.T., M.L., and D.L.; methodology, A.G. and M.W.; investigation, M.T., A.G., and M.W.; resources, M.T.; writing—original draft preparation, M.T.; writing—review and editing, M.T.; funding acquisition, M.T., M.L., D.L., and M.W.

Funding: This research (oxygen isotope measurements) was funded by SYNTHESYS (http://www.synthesys.info/; rant number SE-TAF-2760) which is financed by the European Community—Research Infrastructure Action under the FP7 "Capacities" specific Programme. The NordSIMS facility operates as a Swedish-Icelandic infrastructure of which this is publication # 626. In addition, the Saxonian Geological Survey supported this project.

Acknowledgments: We acknowledge three anonymous reviewers for their constructive comments and questions.

Conflicts of Interest: The authors declare no conflict of interest.

References

1. Breiter, K.; Förster, H.J.; Seltmann, R. Variscan silicic magmatism and related tin-tungsten mineralization in the Erzgebirge-Slavkovsky les metallogenic province. *Mineral. Depos.* **1999**, *34*, 505–521. [CrossRef]
2. Chappell, B.W.; Hine, R. The Cornubian Batholith: An example of magmatic fractionation on a crustal scale. *Resour. Geol.* **2006**, *56*, 203–244. [CrossRef]
3. Breiter, K.; Svojtka, M.; Ackerman, L.; Švecova, K. Trace element composition of quartz from the Variscan Altenberg-Teplice caldera (Krušneé hory/Erzgebirge Mts, Czech Republic/Germany): Insights into the volcano-plutonic complex evolution. *Chem. Geol.* **2012**, *326–327*, 38–50.
4. Förster, H.J.; Tischendorf, G.; Trumbull, R.B.; Gottesmann, B. Late-Collisional granites in the Variscan Erzgebirge, Germany. *J. Petrol.* **1999**, *40*, 1613–1645. [CrossRef]
5. Förster, H.J.; Romer, R.L.; Gottesmann, B.; Tischendorf, G.; Rhede, D. Are the granites of the Aue-Schwarzenberg Zone (Erzgebirge, Germany) a major source for metalliferous ore deposits? A geochemical, Sr-Nd-Pb isotopic, and geochronological study. *J. Mineral. Geochem.* **2009**, *186*, 163–184. [CrossRef]
6. Romer, R.L.; Kroner, U. Sediment and weathering control on the distribution of Paleozoic magmatic tin-tungsten mineralization. *Mineral. Depos.* **2015**, *50*, 327–338. [CrossRef]
7. Wolf, M.; Romer, R.L.; Franz, L.; Lopez-Moro, F.J. Tin in granitic melts: The role of melting temperature and protolith composition. *Lithos* **2018**, *310–311*, 20–30. [CrossRef]
8. Kröner, A.; Willner, A.P.; Hegner, E.; Frischbutter, A.; Hofmann, J.; Bergner, R. Latest Precambrian (Cadomian) zircon ages, Nd isotopic systematics and p-T evolution of granitoid orthogneisses of the Erzgebirge, Saxony and Czech Republic. *Geol. Rundsch.* **1995**, *84*, 437–456. [CrossRef]
9. Schmädicke, E.; Mezger, K.; Cosca, M.A.; Okrusch, M. Variscan Sm-Nd and Ar-Ar ages of eclogite facies rocks from the Erzgebirge, Bohemian massif. *J. Metamorph. Geol.* **1995**, *13*, 537–552. [CrossRef]
10. Schmädicke, E.; Will, T.M.; Ling, X.; Li, X.-H.; Li, Q.-L. Rare peak and ubiquitous post-peak zircon in eclogite: Constraints for the timing of UHP and HP metamorphism in Erzgebirge, Germany. *Lithos* **2018**, *322*, 250–267. [CrossRef]

11. Willner, A.P.; Rötzler, K.; Maresch, W.V. Pressure-Temperature and fluid evolution of quartzo-feldspathic metamorphic rocks with a relic high-pressure, granulite-facies history from the Central Erzgebirge (Saxony, Germany). *J. Petrol.* **1997**, *38*, 307–336. [CrossRef]
12. Mingram, B.; Kröner, A.; Hegner, E.; Krentz, O. Zircon ages, geochemistry, and Nd isotopic systematics of pre-Variscan orthogneisses from the Erzgebirge, Saxony (Germany) and geodynamic interpretation. *Int. J. Earth Sci.* **2004**, *9*, 706–727. [CrossRef]
13. Massonne, H.J.; Kennedy, A.; Nasdala, L.; Theye, Z. Dating of zircon and monazite from diamondiferous quartzofeldspathic rocks of the Saxonian Erzgebirge—Hints at burial and exhumation velocities. *Min. Mag.* **2007**, *71*, 371–389. [CrossRef]
14. Tichomirowa, M.; Berger, H.J.; Koch, E.A.; Belyatski, B.; Götze, J.; Kempe, U.; Nasdala, L.; Schaltegger, U. Zircon ages of high-grade gneisses in the Eastern Erzgebirge (Central European Variscides)—Constraints on origin of the rocks and Precambrian to Ordovician magmatic events in the Variscan foldbelt. *Lithos* **2001**, *56*, 303–332. [CrossRef]
15. Tichomirowa, M.; Whitehouse, M.J.; Nasdala, L. Resorption, growth, solid state recrystallisation, and annealing of granulite facies zircon—A case study from the Central Erzgebirge, Bohemian Massif. *Lithos* **2005**, *82*, 25–50. [CrossRef]
16. Tichomirowa, M.; Sergeev, S.; Berger, H.J.; Leonhardt, D. Inferring protoliths of high-grade metamorphic gneisses of the Erzgebirge using zirconology, geochemistry and comparison with lower-grade rocks from Lusatia (Saxothuringia, Germany). *Contrib. Mineral. Petrol.* **2012**, *164*, 375–396. [CrossRef]
17. Tichomirowa, M.; Whitehouse, M.; Gerdes, A.; Schulz, B. Zircon (Hf, O isotopes) as melt indicator: Melt infiltration and abundant new zircon growth within melt rich layers of granulite-facies lenses versus solid-state recrystallization in hosting amphibolite-facies gneisses (central Erzgebirge, Bohemian Massif). *Lithos* **2018**, *302–303*, 65–68. [CrossRef]
18. Tichomirowa, M.; Käßner, A.; Sperner, B.; Lapp, M.; Leonhardt, D.; Linnemann, U.; Münker, C.; Ovtcharova, M.; Pfänder, J.A.; Schaltegger, U.; et al. Dating multiply overprinted granites: The effect of protracted magmatism and fluid flow on dating systems (zircon U-Pb: SHRIMP/SIMS, LA-ICP-MS, CA-ID-TIMS; and Rb-Sr, Ar-Ar)—Granites from the Western Erzgebirge (Bohemian Massif, Germany). *Chem. Geol.* **2019**, *519*, 11–38. [CrossRef]
19. Rötzler, K.; Plessen, B. The Erzgebirge: A pile of ultrahigh- to low-pressure nappes of Early Paleozoic rocks and their Cadomian basement. In *Pre-Mesozoic Geology of Saxo-Thuringia*; Linnemann, U., Romer, R.L., Eds.; Schweizerbartsche Verlagsbuchhandlung: Stuttgart, Germany, 2010; pp. 253–270.
20. Schmädicke, E. Quartz pseudomorphs after coesite in eclogites from the Saxonian Erzgebirge. *Eur. J. Mineral.* **1991**, *3*, 231–238. [CrossRef]
21. Massonne, H.J. A comparison of evolution of diamondiferous quartz-rich rocks from the Saxonian Erzgebirge and the Kokchetav Massif: Are so-called diamondiferous gneisses magmatic rocks? *Earth Planet. Sci. Lett.* **2003**, *216*, 347–364. [CrossRef]
22. Kröner, A.; Willner, A.P. Time of formation and peak of Variscan HP-HT metamorphism of quartz-feldspar rocks in the central Erzgebirge, Saxony, Germany. *Contrib. Mineral. Petrol.* **1998**, *132*, 1–20. [CrossRef]
23. Tichomirowa, M.; Köhler, R. Discrimination of protolithic versus metamorphic zircon ages in eclogites: Constraints from the Erzgebirge metamorphic core complex (Germany). *Lithos* **2013**, *177*, 436–450. [CrossRef]
24. Rötzler, K.; Schumacher, R.; Maresch, W.V.; Willner, A.P. Characterization and geodynamic implications of contrasting metamorphic evolution in juxtaposed high-pressure units of the Western Erzgebirge (Saxony, Germany). *Europ. J. Mineral.* **1998**, *10*, 261–280. [CrossRef]
25. Kroner, U.; Görz, I. Variscan assemblage of the allochthonous domain of the Saxo-Thuringian Zone—A tectonic model. In *Pre-Mesozoic Geology of Saxo-Thuringia*; Linnemann, U., Romer, R.L., Eds.; Schweizerbart Science Publishers: Stuttgart, Germany, 2010; pp. 271–286.
26. Thomas, R.; Klemm, W. Microthermometric study of silicate melt inclusions in Variscan granites from SE Germany: Volatile contents and entrapment conditions. *J. Petrol.* **1997**, *38*, 1753–1765. [CrossRef]
27. Brause, H.; Eilers, H.; Baumgart, G. *Gravimetrische Übersichtskarte des Freistaates Sachsen 1:400,000, Karte der BOUGER-Schwerestörung*; Sächsisches Landesamt für Umwelt und Geologie: Dresden, Germany, 1993.
28. Baumann, L.; Kuschka, E.; Seifert, T. *Lagerstätten des Erzgebirges*; Enke im Georg Thieme Verlag: Stuttgart, Germany, 2000; p. 300.

29. Laube, G. Geologie des Böhmischen Erzgebirges. Comm. Verl. Fr. Rivnac, Prague. 1887. Available online: https://www.zobodat.at/pdf/Archiv-Boehmen_6_0001-0259.pdf (accessed on 10 December 2019).
30. Lange, H.; Tischendorf, G.; Pälchen, W.; Klemm, I.; Ossenkopf, W. Zur Petrographie und Geochemie der Granite des Erzgebirges. *Geologie* **1972**, *21*, 457–489.
31. Tischendorf, G.; Geisler, M.; Gerstenberger, H.; Budzinski, H.; Vogler, P. Geochemistry of Variscan granites of the Westerzgebirge Vogtland region—An example of tin deposit-generating granites. *Chemie der Erde* **1987**, *46*, 213–235.
32. Förster, H.J. Die Variszischen Granite des Erzgebirges und Ihre Akzessorischen Minerale. Habilitation Thesis, TU Bergakademie Freiberg, Freiberg, Germany, 1998.
33. Tischendorf, G. *Silicic Magmatism and Metallogenesis of the Erzgebirge*; Central Institute for Physics of the Earth: Potsdam, Germany, 1989; p. 316.
34. Kempe, U.; Bombach, K.; Matukov, D.; Schlothauer, T.; Hutschenreuter, J.; Wolf, D.; Sergeev, S. Pb/Pb and U/Pb zircon dating of subvolcanic rhyolite as a time marker for Hercynian granite magmatism and Sn mineralisation in the Eibenstock granite, Erzgebirge, Germany: Considering effects of zircon alteration. *Mineral. Depos.* **2004**, *39*, 646–669. [CrossRef]
35. Förster, H.J.; Gottesmann, B.; Tischendorf, G.; Siebel, W.; Rhede, D.; Seltmann, R.; Wasternack, J. Permo-Carboniferous subvolcanic rhyolitic dikes in the western Erzgebirge/Vogtland, Germany: A record of source heterogeneity of post-collisional felsic magmatism. *J. Mineral. Geochem.* **2007**, *183*, 123–147. [CrossRef]
36. Förster, H.J.; Romer, R.L. Carboniferous magmatism. In *Pre-Mesozoic Geology of Saxo-Thuringia*; Linnemann, U., Romer, R.L., Eds.; Schweizerbartsche Verlagsbuchhandlung: Stuttgart, Germany, 2010; pp. 287–310.
37. Förster, H.J.; Tischendorf, G.; Seltmann, R.; Gottesmann, B. Die variszischen Granite des Erzgebirges: Neue Aspekte aus stofflicher Sicht. *Z. Geol. Wiss.* **1998**, *26*, 31–60.
38. Förster, H.J.; Tischendorf, G. Compositional heterogeneity of silicic magmatic rocks from the German Variscides. *Z. Geol. Wiss.* **1996**, *24*, 467–482.
39. Breiter, K. Nearly contemporaneous evolution of the A- and S-type fractionated granites in the Krušné hory/Erzgebirge Mts., Central Europe. *Lithos* **2012**, *151*, 105–121. [CrossRef]
40. Stemprok, M.; Dolejš, D.; Müller, A.; Seltmann, R. Textural evidence of magma decompression, devolatilization and disequilibrium quenching: An example from the Western Krušné hory/Erzgebirge granite pluton. *Contrib. Mineral. Petrol.* **2008**, *155*, 93–109. [CrossRef]
41. Thomas, R.; Davidson, P.; Rhede, D.; Leh, M. The miarolitic pegmatites from the Königshain: A contribution to understanding the genesis of pegmatites. *Contrib. Mineral. Petrol.* **2009**, *157*, 505–523. [CrossRef]
42. Webster, J.D.; Thomas, R.; Rhede, D.; Förster, H.J.; Seltmann, R. Melt inclusions in quartz from an evolved peraluminous pegmatite: Geochemical evidence for strong tin enrichment in fluorine-rich and phosphorus-rich residual liquids. *Geochim. Cosmochim. Acta* **1997**, *61*, 2589–2604. [CrossRef]
43. Webster, J.; Thomas, R.; Förster, H.J.; Seltmann, R.; Tappen, C. Geochemical evolution of halogen-enriched granite magmas and mineralizing fluids of the Zinnwald tin-tungsten mining district, Erzgebirge, Germany. *Mineral. Depos.* **2004**, *39*, 452–472. [CrossRef]
44. Thomas, R.; Förster, H.J.; Rickers, K.; Webster, J.D. Formation of extremely F-rich hydrous melt fractions and hydrothermal fluids during differentiation of highly evolved tin-granite magmas: A melt/fluid inclusion study. *Contrib. Mineral. Petrol.* **2005**, *148*, 582–601. [CrossRef]
45. Dolejš, D.; Baker, D.R. Thermodynamic analysis of the system Na_2O-K_2O-CaO-Al_2O_3-SiO_2-H_2O-F_2O_{-1}: Stability of fluorine-bearing minerals in felsic igneous suites. *Contrib. Mineral. Petrol.* **2004**, *146*, 762–778. [CrossRef]
46. Müller, A.; Breiter, K.; Seltmann, R.; Pécskay, Z. Quartz and feldspar zoning in the eastern Erzgebirge volcano-plutonic complex (Germany, Czech Republic): Evidence of multiple magma mixing. *Lithos* **2005**, *80*, 201–227. [CrossRef]
47. Romer, R.L.; Meixner, A.; Förster, H.J. Lithium and boron in late-orogenic granites—Isotopic fingerprints for the source of crustal melts? *Geochim. Cosmochim. Acta* **2014**, *131*, 98–114. [CrossRef]
48. Stemprok, M.; Holub, F.V.; Novak, J.K. Multiple magmatic pulses of the Eastern Volcano-Plutonic Complex, Krušné hory/Erzgebirge batholith, and their phosphorus contents. *Bull. Geosci.* **2003**, *78*, 277–296.
49. DePaolo, D.J. Neodymium isotopes in the Colorado Front Range and crust–mantle evolution in the Proterozoic. *Nature* **1981**, *291*, 193–196. [CrossRef]

50. Gerdes, A.; Zeh, A. Combined U-Pb and Hf isotope LA-(MC)ICP-MS analyses of detrital zircons: Comparison with SHRIMP and new constraints for the provenance and age of an Armorican metasediment in Central Germany. *Earth Planet. Sci. Lett.* **2006**, *249*, 47–61. [CrossRef]
51. Sláma, J.; Košler, J.; Condon, D.J.; Crowley, J.L.; Gerdes, A.; Hanchar, J.M.; Horstwood, M.S.A.; Morris, G.A.; Nasdala, L.; Norberg, N.; et al. Plesovice zircon—A new natural reference material for U-Pb and Hf isotopic microanalysis. *Chem. Geol.* **2008**, *249*, 1–35. [CrossRef]
52. Whitehouse, M.J.; Nemchin, A.A. High precision, high accuracy measurement of oxygen isotopes in a large lunar zircon by SIMS. *Chem. Geol.* **2009**, *261*, 32–42. [CrossRef]
53. Wiedenbeck, M.; Hanchar, J.; Peck, W.H.; Sylvester, P.; Valley, J.; Whitehouse, M.; Kronz, A.; Morishita, Y.; Nasdala, L. Further characterization of the 91500 zircon crystal. *Geostand. Geoanal. Res.* **2004**, *28*, 9–39. [CrossRef]
54. Hinton, R.W.; Upton, B.G.J. The chemistry of zircon: Variations within and between large crystals from syenites and alkali basalt xenoliths. *Geochim. Cosmochim. Acta* **1991**, *55*, 3278–3302. [CrossRef]
55. Watson, E.B.; Harrison, T.M. Zircon saturation revisited: Temperature and composition effects in a variety of crustal magma types. *Earth Planet. Sci. Lett.* **1983**, *64*, 295–304. [CrossRef]
56. Jung, S.; Pfänder, J.A. Source composition and melting temperatures of orogenic granitoids: Constraints from CaO/Na_2O, Al_2O_3/TiO_2 and accessory mineral saturation thermometry. *Eur. J. Mineral.* **2007**, *19*, 859–870. [CrossRef]
57. Bouvier, A.; Vervoort, J.D.; Patchett, P.J. The Lu-Hf and Sm-Nd isotopic composition of CHUR: Constraints from unequilibrated chondrites and implications for the bulk composition of terrestrial planets. *Earth Planet. Sci. Lett.* **2008**, *273*, 48–57. [CrossRef]
58. Watson, E.B.; Wark, D.A.; Thomas, J.B. Crystallization thermometers for zircon and rutile. *Contrib. Mineral. Petrol.* **2006**, *151*, 413–433. [CrossRef]
59. Chen, R.-X.; Zheng, Y.-F. Metamorphic zirconology of continental subduction zones. *J. Asian Earth Sci.* **2017**, *145*, 149–176. [CrossRef]
60. Linnemann, U.; Gerdes, A.; Hofmann, M.; Marko, L. The Cadomian orogen: Neoproterozoic to Early Cambrian crustal growth and orogenic zoning along the periphery of the West African Craton—Constraints from U-Pb zircon ages and Hf isotopes (Schwarzburg Antiform, Germany). *Precamb. Res.* **2014**, *244*, 236–278. [CrossRef]
61. Farina, E.; Stevens, G.; Gerdes, A.; Frei, D. Small-scale Hf isotopic variability in the Peninsula pluton (South Africa): The processes that control inheritance of source $^{176}Hf/^{177}Hf$ diversity in S-type granites. *Contrib. Mineral. Petrol.* **2014**, *168*, 1065. [CrossRef]
62. Bindemann, I.N.; Bekker, A.; Zakharov, D.O. Oxygen isotope persppective on crustal evolution on early Earth: A record of Precambrian shales with emphasis on Paleoproterozoic glaciations and Great Oxygenation Event. *Earth Planet. Sci. Lett.* **2016**, *437*, 101–113. [CrossRef]
63. Massonne, H.J. Pre-conference field trip: Erzgebirge Mountains, Germany; 4–5 August 2011. In Proceedings of the 9th International Eclogite Conference 2011, 6–9 August 2011 Marianzke Lazne, Czech Republic, GeoLines 23, Prague, Czech Republic. Faryad, S.W., Medaris, L.G., Eds.; pp. 29–59. Available online: http://geolines.gli.cas.cz/index.php?id=volume23 (accessed on 10 December 2019).
64. Tichomirowa, M.; Leonhardt, D. New age determinations (Pb/Pb zircon evaporation, Rb/Sr) on the granites from Aue-Schwarzenberg and Eibenstock, Western Erzgebirge, Germany. *Z. Geol. Wiss.* **2010**, *38*, 99–123.
65. Mingram, B.; Rötzler, K. Geochemische, petrologische und geochronologische Untersuchungen im Erzgebirgskristrallin—Rekonstruktion eines Krustenstapels. *Schriftenr. Geowiss.* **1999**, *9*, 80.
66. Nägler, T.F.; Schäfer, H.J.; Gebauer, D. Evolution of the Western European continental crust: Implications from Nd and Pb isotopes in Iberian sediments. *Chem. Geol.* **1995**, *121*, 345–357. [CrossRef]
67. Simien, F.; Mattauer, M.; Allegre, C.J. Nd isotopes in the stratigraphical record of the Montagne Noire (French Massif Central): No significant Palaeozoic juvenile inputs, and pre-Hercynian paleogeography. *J. Geol.* **1999**, *107*, 87–97. [CrossRef]
68. Vila, M.; Pin, C. Geochemistry and Nd isotope signature of the Collserola Range Palaeozoic succesion (NE Iberia): Gondwana heritage and pre-Mesozoic geodynamic evolution. *Geol. Mag.* **2016**, *153*, 643–662. [CrossRef]
69. Clemens, J.D. S-type granitic magmas-petrogenetic issues, models and evidence. *Earth-Sci. Rev.* **2003**, *61*, 1–18. [CrossRef]

70. Wang, L.X.; Ma, C.Q.; Zhang, C.; Zhang, J.Y.; Marks, M.A.W. Genesis of leucogranite by prolonged fractional crystallization: A case study of the Mufushan complex, South China. *Lithos* **2014**, *206–207*, 147–163. [CrossRef]
71. Clemens, J.D.; Stevens, G. What controls chemical variation in granitic magmas? *Lithos* **2012**, *134–135*, 317–329. [CrossRef]
72. Villaros, A.; Stevens, G.; Moyen, J.F.; Buick, I.S. The trace element composition of S-type granites: Evidence for disequilibrium melting and accessory phase entrainment in the source. *Contrib. Mineral. Petrol.* **2009**, *158*, 543–561. [CrossRef]
73. Clemens, J.D. Element concentrations in granitic magmas: Ghost of textures past? *J. Geol. Soc. Lond.* **2014**, *171*, 13–19. [CrossRef]
74. Boehnke, P.; Bruce-Watson, E.; Trail, D.; Harrison, T.M.; Schmitt, A.K. Zircon saturation re-visited. *Chem. Geol.* **2013**, *351*, 324–334. [CrossRef]
75. Pupin, J.P. Zircon and granite petrology. *Contrib. Mineral. Petrol.* **1980**, *73*, 207–220. [CrossRef]
76. Schiller, D.; Finger, F. Application of Ti-in-zircon thermometry to granite studies: Problems and possible solutions. *Contrib. Mineral. Petrol.* **2019**, *174*, 51. [CrossRef]
77. Lackey, J.S.; Valley, J.W.; Chen, J.H.; Stockli, D.F. Dynamic Magma Systems, Crustal Recycling, and Alteration in the Central Sierra Nevada Batholith: The Oxygen Isotope Record. *J. Petrol.* **2008**, *49*, 1397–1426. [CrossRef]
78. Chappell, B.W.; White, A.J.R. Two contrasting granite types. *Pac. Geol.* **1974**, *8*, 173–174.
79. Werner, O.; Lippolt, H.J. White mica $^{40}Ar/^{39}Ar$ ages of the Erzgebirge metamorphic rocks: Simulating the chronological results by a model of Variscan crustal imbrication. In *Orogenic Processes: Quantification and Modelling in the Variscan Belt*; Franke, W., Haak, V., Oncken, O., Tanner, D., Eds.; Geological Society London Special Publications: London, UK, 2000; pp. 323–336.
80. Zack, T.; Luvizottow, G.L. Application of rutile thermometry to eclogites. *Mineral. Petrol.* **2006**, *88*, 69–85. [CrossRef]
81. Wang, R.C.; Xie, L.; Chen, J.; Yu, A.; Wang, L.; Lu, J.; Zhu, J. Tin-carrier minerals in metaluminous granites of the western Nanling Range (southern China): Constraints on processes of tin mineralization in oxidized granites. *J. Asian Earth Sci.* **2013**, *74*, 361–372. [CrossRef]
82. Carocci, E.; Marignac, C.; Cathelineau, M.; Truche, L.; Andreï Lecomte, A.; Pinto, F. Rutile from Panasqueira (Central Portugal): An Excellent Pathfinder for Wolframite Deposition. *Minerals* **2019**, *9*, 9. [CrossRef]
83. Luvizotto, G.L.; Zack, T.; Meyer, H.P.; Ludwig, T.; Triebold, S.; Kronz, A.; Münker, C.; Stockli, D.F.; Prowatke, A.; Klemme, S.; et al. Rutile crystals as potential trace element and isotope mineral standards for microanalysis. *Chem. Geol.* **2009**, *261*, 346–369. [CrossRef]
84. Neves, L.J.P.F. Trace element content and partitioning between biotite and muscovite of granitic rocks: A study in the Viseu region (Central Portugal). *Eur. J. Mineral.* **1997**, *9*, 849–857. [CrossRef]
85. Tischendorf, G.; Förster, H.J.; Gottesmann, B. Minor- and trace-element composition of trioctahedral micas: A review. *Mineral. Mag.* **2001**, *65*, 249–276. [CrossRef]
86. Du Bray, E.A. Garnet compositions and their use as indicators of peraluminous granitoid petrogenesis—Southeastern Arabian Shield. *Contrib. Mineral. Petrol.* **1988**, *100*, 205–212. [CrossRef]
87. Anders, E.; Grevesse, N. Abundances of elements: Meteoric and solar. *Geochim. Cosmochim. Acta* **1989**, *53*, 44–451. [CrossRef]
88. Rudnick, R.L.; Gao, S. Composition of the continental crust. In *Treatise on Geochemistry*, 2nd ed.; Holland, H.D., Turekian, K.K., Eds.; Elsevier: Amsterdam, The Netherlands, 2014; Volume 4, pp. 1–51.